

Seasonal characteristics, formation mechanisms and source origins of PM_{2.5} in two megacities in Sichuan Basin, China

Huanbo Wang^{1,2}, Mi Tian¹, Yang Chen¹, Guangming Shi¹, Yuan Liu¹, Fumo Yang^{1,2,3,4*}, Leiming Zhang⁵, Liqun Deng⁶, Jiayan Yu⁷, Chao Peng¹, and Xuyao Cao¹

¹Research Center for Atmospheric Environment, Chongqing Institute of Green and Intelligent Technology, Chinese Academy of Sciences, Chongqing, 400714, China

²School of Urban Construction and Environmental Engineering, Chongqing University, Chongqing, 400044, China

³Center for Excellence in Regional Atmospheric Environment, Institute of Urban Environment, Chinese Academy of Sciences, Xiamen, 361021, China

⁴Yangtze Normal University, Chongqing, 408100, China

⁵Environment and Climate Change Canada, Toronto, Canada

⁶Sichuan Academy of Environmental Sciences, Chengdu, 610041, China

⁷Chongqing Environmental Monitoring Center, Chongqing 401147, China

Correspondence to: Fumo Yang (fmyang@cigit.ac.cn)

1 **Abstract.** To investigate the characteristics of PM_{2.5} and its major chemical components, formation
2 mechanisms, and geographical origins in the two megacities, Chengdu (CD) and Chongqing (CQ), in
3 Sichuan Basin of southwest China, daily PM_{2.5} samples were collected simultaneously at one urban site
4 in each city for four consecutive seasons from autumn 2014 to summer 2015. Annual mean
5 concentrations of PM_{2.5} were 67.0 ± 43.4 and $70.9 \pm 41.4 \mu\text{g m}^{-3}$ at CD and CQ, respectively. Secondary
6 inorganic aerosols (SNA) and organic matter (OM) accounted for 41.1% and 26.1% of PM_{2.5} mass at
7 CD, and 37.4% and 29.6% at CQ, respectively. Seasonal variations of PM_{2.5} and major chemical
8 components were significant, usually with the highest mass concentration in winter and the lowest in
9 summer. Daily PM_{2.5} concentration exceeded the national air quality standard on 30% of the sampling
10 days at both sites, and most of the pollution events were at the regional scale within the basin formed
11 under stagnant meteorological conditions. The concentrations of carbonaceous components were higher
12 at CQ than CD, likely partially caused by emissions from the large amount of motorcycles and spraying
13 process during automobile production in CQ. Heterogeneous reactions probably played an important
14 role in the formation of SO₄²⁻, while both homogeneous and heterogeneous reactions contributed to the
15 formation of NO₃⁻. Geographical origins of emissions sources contributing to high PM_{2.5} masses at both
16 sites were identified to be mainly distributed within the basin based on potential source contribution
17 function (PSCF) analysis.

18

19 **1 Introduction**

20 Fine particles (PM_{2.5}, particulate matter with an aerodynamic diameter smaller than 2.5 µm) have
21 adverse effects on human health (Anderson et al., 2012; Lepeule et al., 2012; Taus et al., 2008),
22 deteriorate air quality (Zhang et al., 2008; Paraskevopoulou et al., 2015), reduce atmospheric visibility
23 (Fu et al., 2016; Cao et al., 2012; Baumer et al., 2008), impact climate (Ramanathan and Feng,
24 2009; Hitztenberger et al., 1999; Mahowald, 2011), and affect ecosystem (Larssen et al., 2006). In the past
25 two decades, China has experienced serious PM_{2.5} pollution due to the rapidly increasing energy
26 consumption through economic development, industrialization and urbanization (Tie and Cao, 2009).
27 The National Ambient Air Quality Standards (NAAQS) for PM_{2.5} was promulgated by the Chinese
28 government in 2012, and strict strategies have been implemented nationwide, e.g. controlling SO₂
29 emissions by installing desulphurization system in coal-fired power plants and conversion of fuel to
30 natural gas (Lu et al., 2011), mitigating NO_x emissions through traffic restrictions, and reducing
31 biomass burning through straw shredding. Despite these efforts, there are still many cities that have not
32 yet met the current NAAQS (Tao et al., 2017). According to the ‘2013-2015 Reports on the State of
33 Environment of China’, annual mean concentration of PM_{2.5} in 74 major cities across China was 72, 64,
34 and 50 µg m⁻³ in 2013, 2014 and 2015, respectively, and only 4.1%, 12.2% and 22.5% of the monitored
35 cities met the NAAQS (35 µg m⁻³).

36 Previous studies showed that Beijing-Tianjin-Hebei area (BTH), Yangtze River Delta (YRD), Pearl
37 River Delta (PRD), and Sichuan Basin were the four main regions in China with severe aerosol
38 pollution (Tao et al., 2017). While many studies have been conducted in BTH, PRD and YRD regions
39 to understand the general characteristics of PM_{2.5} and its chemical components, formation mechanism,
40 and sources (Ji et al., 2016; Li et al., 2015; Quan et al., 2015; Tan et al., 2016; Yang et al., 2015; Zhang et
41 al., 2013; Zhao et al., 2015; Zhao et al., 2013a; Cheng et al., 2015; Zheng et al., 2015a; Yang et al., 2011a),
42 only a few studies have focused on the Sichuan Basin (Tao et al., 2014; Tian et al., 2013; Yang et al.,
43 2011b). Covering an area of 260,000 km² and with a population of around 100 million, the Sichuan
44 Basin is the most populated basin in China. It is a subtropical expanse of low hills and plains and is
45 completely encircled by high mountains and plateaus. It is also characterized by persistently high
46 relative humidity and extremely low wind speeds all the year-round (Guo et al., 2016; Chen and Xie,
47 2013). The characteristics of PM_{2.5} in the Sichuan Basin are supposed to be very different from those in
48 eastern coastal China (i.e. PRD and YRD) and North China Plain (i.e. BTH) due to the special

topography and meteorological conditions, besides emission sources, in the basin. Furthermore, the terrain in the two megacities is also distinct from each other significantly, i.e., Chongqing is a mountainous city lying on the eastern margin of the basin while Chengdu is a flat city on the western margin of the basin. Therefore, there is a great interest in comparing the chemical components of PM_{2.5} and characterizing pollution episodes between the two cities.

The present study aims to fill this gap by measuring chemically-resolved PM_{2.5} in Chengdu and Chongqing in four consecutive seasons during 2014-2015. The main objectives are to: (1) characterize PM_{2.5} mass and major chemical components in urban environments of Chengdu and Chongqing; (2) compare PM_{2.5} chemical compositions under different pollution levels and identify major chemical components responsible for long-lasting PM_{2.5} pollution episodes in winter; (3) explore the possible formation mechanism of the secondary aerosols; and (4) reveal the geographical source regions contributing to the high PM_{2.5} levels through PSCF analysis. Knowledge gained in this study provides scientific basis for making future emission control policies aiming to alleviating heavy PM_{2.5} pollution in this unique basin.

2 Methodology

2.1 Sampling sites

PM_{2.5} samples were collected at two urban sites, one in Chengdu and another in Chongqing, the two largest cities in Sichuan Basin, southwest China. The two sampling sites are located 260 km apart (Fig. 1). The sampling site in Chengdu (CD) is located on the roof of a sixth floor building in the Sichuan Academy of Environmental Science (104°4' E, 30°37' N) with no large surrounding industries but heavy traffic. The closest main road (Renmin South road of Chengdu) is about 20 m east of the sampling site. The sampling site in Chongqing (CQ) is located on the rooftop of Chongqing Monitoring Center (106°30' E, 29°37' N). The highway G50 is 250 m away from this sampling site. The two selected sampling sites are considered to represent typical urban environments in their respective cities (Tao et al., 2014; Chen et al., 2017).

2.2 Sample collection

Daily (23-h) integrated PM_{2.5} samples were collected in four months, each in a different season: autumn (23 October to 18 November, 2014), winter (6 January to 2 February, 2015), spring (2 to 29 April, 2015), and summer (2 to 30 July, 2015). At both sites, PM_{2.5} samples were collected in parallel on Teflon filters (Whatman Corp., 47 mm) and quartz filters (Whatman Corp., 47 mm). At CD site, PM_{2.5}

sampling was carried out using a versatile air pollutant sampler (Wang et al., 2017). One channel was used to load PM_{2.5} sample on Teflon filter for mass and trace elements analysis and the other one was equipped with quartz filter for water-soluble inorganic ions and carbonaceous components analysis. The sampler was running at 15 L min⁻¹ for each channel. At CQ site, a low-volume aerosol sampler (BGI Corp., from Omni, USA) operating at a flow rate of 5 L min⁻¹ was used to collect PM_{2.5} samples on Teflon filter, and another sampler (Thermo Scientific Corp. Partisol 2000i, USA) with a flow rate of 16.7 L min⁻¹ was used to collect PM_{2.5} samples on quartz filter. A total of 112 samples and 8 field blanks, nearly equally distributed in the four seasons, were collected at each site during the campaign. In addition, three lab blank filters in each campaign were stored in a clean Petri slides in the dark and analysed in the same ways as the collected samples to evaluate the background contamination.

Before sampling, all the quartz filters were preheated at 450°C for 4 h to remove the organic compounds. All sampled filters were stored in clean Petri slides in the dark and at -18°C until analysis to prevent the evaporation of volatile compounds. Before and after sample collection, all the Teflon filters were weighted at least three times using an microbalance (Sartorius, ME 5-F, Germany) after their stabilization for 48 h under controlled conditions (temperature: 20~23°C, relative humidity: 45~50%). Differences among replicate weights were mostly less than 15 µg for each sample.

2.3 Chemical analysis

For the analysis of water-soluble inorganic ions, a quarter of each quartz filter was first extracted using ultrapure water in an ultrasonic bath for 30 min, and then filtered through a 0.45 µm pore syringe filter. Anions (SO₄²⁻, NO₃⁻ and Cl⁻) and cations (Na⁺, NH₄⁺, K⁺, Mg²⁺ and Ca²⁺) were determined using ion chromatograph (Dionex Corp., Dionex 600, USA). Anions were separated using AS11-HC column with 30 mM KOH as an eluent at a flow rate of 1.0 ml min⁻¹. Cations were determined using CS12A column with 20 mM MSA (methanesulfonic acid) at a flow rate of 1.0 ml min⁻¹. Individual standard solutions of all investigated anions and cations (1000 mg L⁻¹, o2si, USA) were diluted to construct the calibration curves. The correlation coefficients of the linear regression of the standard curves were all above 0.999. Field blanks were prepared and analyzed together with the samples and then subtracted from the samples. The concentrations of the water-soluble inorganic ions in the field blanks were in the range of 0.008-0.13 µg m⁻³. The relative standard deviation of each ion was better than 8% for the reproducibility test.

Organic carbon (OC) and elemental carbon (EC) were measured by thermal-optical reflectance

(TOR) method using a DRI OC/EC analyzer (Atmoslytic Inc., USA). The methodology for OC/EC analysis was based on TOR method as described in Chow et al. (2007). For calibration and quality control, measurement with filter blank, standard sucrose solution and replicate analysis were performed. Blank corrections were performed by subtracting the blank values from the sampled ones. The concentration of EC in field blanks was zero while OC was below $0.7 \mu\text{g C cm}^{-2}$. The repeatability was better than 15%.

The elements including Al, Si, Ca, Fe, and Ti were analyzed on Teflon filter using X-ray fluorescence analyzer (Epsilon 5ED-XRF, PAN'alytical Corp., Netherlands), the QA/QC procedures of the XRF analysis have been described in Cao et al. (2012). The gaseous species were continuously measured by a set of online gas analyzers, including EC9850 SO₂ analyzer, 9841 NO/NO₂/NO_x analyzer, 9830 CO analyzer, and 9810 O₃ analyzer (Ecotech Corp., Australia) at CD, and Thermo 42i NO/NO₂/NO_x analyzer, 43i SO₂ analyzer, 48i CO analyzer, and 49i O₃ analyzer (Thermo Scientific Corp., USA) at CQ. The mass concentrations of PM_{2.5} were automatically measured by online particulate monitor instruments (BAM1020, Met one Corp., USA, at CD and 5030 SHARP, Thermo Scientific Corp, USA, at CQ). Hourly meteorological parameters, including ambient temperature (T), relative humidity (RH), wind speed (WS) and direction, barometric pressure (P), and solar radiation (SR) were obtained from an automatic weather station (Lufft Corp. WS501, Germany) at each site. Hourly precipitation data were recorded at the nearest weather station operated by China Meteorology Administration (<http://www.weather.com.cn/>). Planetary boundary layer height (PBLH) was obtained from the HYSPLIT model (<http://ready.arl.noaa.gov/HYSPLIT.php>).

2.4 Data analysis

The EC-tracer method has been widely used to estimate SOC (Turpin and Lim, 2001;Castro et al., 1999), which can be expressed as

$$\text{POC}=(\text{OC/EC})_{\text{prim}} \times \text{EC} \quad (1)$$

$$\text{SOC}=\text{OC}-\text{POC} \quad (2)$$

Where POC, SOC and OC represent the estimated primary OC, secondary OC and measured total OC, respectively. (OC/EC)_{min} was simplified as the (OC/EC)_{prim} to estimate SOC in this study. (OC/EC)_{min} was 2.4, 2.6, 1.6 and 2.2 in autumn, winter, spring and summer at CD, respectively, and 1.9, 2.8, 1.1 and 1.5 at CQ. The estimated SOC was only an approximation with uncertainties, e.g., from influence of biomass burning (Ding et al., 2012).

The coefficient of divergence (COD) has been used to evaluate the spatial similarity of chemical compositions at different sites (Wongphatarakul et al., 1998; Qu et al., 2015), which is defined as

$$COD_{jk} = \sqrt{\frac{1}{p} \sum_1^p \left(\frac{x_{ij} - x_{ik}}{x_{ij} + x_{ik}} \right)^2} \quad (3)$$

Where x_{ij} and x_{ik} represent the average concentration for a chemical component i at site j and k , respectively, p is the number of chemical components. Generally, a COD value lower than 0.2 indicates a relatively similarity of spatial distribution.

2.5 Geographical origins of PM_{2.5}

72-h air mass back trajectories were generated based on the Hybrid Single Particle Lagrangian Integrated Trajectory (HYSPLIT) model using 0.5°×0.5° meteorological data for the period of October 2014 to July 2015 when PM_{2.5} measurements were made at both sites. Four trajectories at 04:00, 10:00, 16:00, and 22:00 UTC every day with the starting height of 300 m above ground level were calculated (Squizzato and Masiol, 2015).

PSCF is substantially a conditional probability that trajectories with pollutant concentrations larger than a given criterion passed through a grid cell (i,j) (Ashbaugh et al., 1985; Polissar et al., 1999), that means a grill cell (i,j) with high PSCF values are mostly potential source locations of pollutants. PSCF is defined as follows,

$$PSCF_{ij} = \frac{m_{ij}}{n_{ij}} \quad (4)$$

Where n_{ij} is the total number of endpoints falling in the grid cell (i,j) and m_{ij} denotes the number of endpoints that are associated with samples exceeding the threshold criterion in the same cell. To reduce the PSCF uncertainties associated with small n_{ij} values, weighting function was adopted as follows,

$$W_{ij} = \begin{cases} 1.0 & 3n_{ave} < n_{ij} \\ 0.7 & 1.5n_{ave} < n_{ij} \leq 3n_{ave} \\ 0.42 & n_{ave} < n_{ij} \leq 1.5n_{ave} \\ 0.2 & n_{ij} \leq n_{ave} \end{cases} \quad (5)$$

Where n_{ave} is the average number of endpoints in each grid cell.

The trajectories coupled with daily pollutants concentrations were used for PSCF analysis, with the threshold criterion in PSCF analysis being set at the upper 50% of PM_{2.5} and other pollutants. The trajectory covered area was in the range of 20-45° N and 90-120° E and divided into 0.5°×0.5° grid cells.

164 **3 Results and discussion**

165 **3.1 PM_{2.5} mass concentration and chemical composition**

166 **3.1.1 Overview**

167 Table 1 presents seasonal and annual mean concentrations of PM_{2.5} and its major chemical components
168 at CD and CQ during the sampling periods. Daily PM_{2.5} ranged from 11.6 to 224.7 $\mu\text{g m}^{-3}$ with annual
169 average being $67.0 \pm 43.4 \mu\text{g m}^{-3}$ at CD and $70.9 \pm 41.4 \mu\text{g m}^{-3}$ at CQ, which were about two times the
170 NAAQS annual limit. Secondary inorganic aerosol (SNA, the sum of SO_4^{2-} , NO_3^- and NH_4^+) and
171 carbonaceous species together represented more than 70% of PM_{2.5} mass at both sites (Fig. 2). The
172 annual mean concentrations of SNA were $27.6 \mu\text{g m}^{-3}$ at CD and $26.5 \mu\text{g m}^{-3}$ at CQ, contributing 41.1%
173 and 37.4% to PM_{2.5} mass, respectively. SO_4^{2-} , NO_3^- and NH_4^+ accounted for 16.8%, 13.6% and 10.8%,
174 respectively, of PM_{2.5} mass at CD, and 17.2%, 10.9% and 9.2%, respectively, at CQ. Organic matters
175 (OM), estimated from OC using a conversion factor of 1.6 to account for other elements presented in
176 organic compounds (Turpin and Lim, 2001), were the most abundant species in PM_{2.5}, accounting for
177 26.1% and 29.6% of PM_{2.5} mass at CD and CQ, respectively. In contrast, EC only comprised of around
178 6% at both sites. The annual mean concentrations of OC and EC were 20% and 25%, respectively, and
179 were higher at CQ than CD. The annual mean concentration of fine soil (FS), calculated by summing
180 the oxides of major crustal elements, i.e., Al_2O_3 , SiO_2 , CaO , FeO , Fe_2O_3 , and TiO_2 (Huang et al., 2014),
181 was $6.7 \mu\text{g m}^{-3}$ (9.5% of PM_{2.5} mass) at CQ. It is noted that this was about two times that at CD ($3.8 \mu\text{g}$
182 m^{-3} , 5.7% of PM_{2.5} mass). The minor components such as K^+ and Cl^- constituted less than 5% of PM_{2.5}.
183 The unaccounted portions of PM_{2.5} reached 18.3% at CD and 15.3% at CQ, which were likely related to
184 the uncertainties in the multiplication factors used for estimating OM and FS, other unidentified species,
185 and measurement uncertainties.

186 **3.1.2 Seasonal variations**

187 Figure 3 shows the seasonal variations in mass concentrations of PM_{2.5} and its major chemical
188 components at CD and CQ. Seasonal variations of any pollutants were influenced by the seasonal
189 variations in source emission intensities, atmospheric processes and meteorological conditions. Unlike in
190 northern China, there were no extensive coal combustion or wood burning for domestic heating in winter
191 due to the warm temperature (around 10°C on average) in the Sichuan Basin, hence atmospheric processes
192 and meteorological conditions played vital roles in the seasonal variations of PM_{2.5}. On a seasonal basis,
193 PM_{2.5} mass was the highest in winter at both CD and CQ, which was 1.8-2.5 times of those in the other

seasons. In contrast, its seasonal differences among the other three seasons were generally small, i.e., less than 40%. Stagnant air conditions with frequent calm winds and low planetary boundary layer heights were the major causes of the highest PM_{2.5} mass in winter (Table 1) (Liao et al., 2017; Chen and Xie, 2013; Li et al., 2017b).

All the major PM_{2.5} components except FS followed the seasonal pattern of PM_{2.5} mass with subtle differences. The highest FS concentrations were observed in spring at both sites. The relatively high wind speed and lower RH in spring were conducive for re-suspension of crustal dust and resulted in higher FS concentrations. In addition, frequent spring dust storms originated in the northwestern China was able to reach Sichuan Basin via long-rang transport, and caused the elevated FS concentrations (Chen et al., 2015; Tao et al., 2013). The highest contributions from FS to PM_{2.5} mass was more than 10%, appeared in spring at both sites. The majority of PM_{2.5} components showed a summer minimum, which was caused by high planetary boundary layer height favoring pollutants dispersion and abundant precipitation favoring wet scavenging (Table 1). One exception was SO₄²⁻, which had a minimum in spring at CD and in autumn at CQ, likely due to the enhanced photochemical reactions associated with high temperature and strong solar radiation in summer. High O₃ concentrations in summer also supported this seasonal trend. It is also noted that the seasonal variations of NO₃⁻ were much larger than those of SO₄²⁻ and NH₄⁺. SO₄²⁻ and SO₂ showed similar seasonal trends, with their concentrations 1.4-2.0 times higher in winter than in the other seasons (Table 1). In contrast, the seasonal variations of NO₃⁻ were much larger than that of NO₂, e.g., while the concentrations of NO₂ were 1.2-1.6 times higher in winter than in the other seasons, those of NO₃⁻ were 9.6 times higher in winter than in summer at CQ. Thus, seasonal variations of SO₂ and NO_x emissions were comparable, but the atmospheric chemical processes caused the much larger seasonal variations in NO₃⁻. The concentration of NO₃⁻ could be enhanced in winter under high RH through heterogeneous aqueous processes and decreased in summer due to volatility of NH₄NO₃ under high temperature, which increased the seasonal differences in NO₃⁻ concentrations between winter and summer (Pathak et al., 2009; Quan et al., 2015; Squizzato et al., 2013). In addition, thermodynamically driven behavior of NH₄NO₃ was another factor for the lower NO₃⁻ concentrations in summer (Wang et al., 2016; Kuprov et al., 2014). As shown in Fig. 2, the seasonal average contributions of SNA to PM_{2.5} only varied within a small range from 39.5% to 43.2% at CD, whereas in a relatively larger range from 31.0% in summer to 37.1-41.5% in the other seasons at CQ. The smaller contribution in summer at CQ was mainly due to the lower NO₃⁻ concentrations. At

both CD and CQ, NO_3^- and NH_4^+ showed the highest contributions in winter and the lowest ones in summer, whereas an opposite trend was found for SO_4^{2-} . Both OC and EC exhibited the highest concentrations in winter at CD and CQ, around 1.9-3.1 times of those in the other seasons. SOC was also the highest in winter at both sites, similarly to what observed for OC, which can be partly explained by the enhanced condensation process forming SOC under low temperature (Sahu et al., 2011; Cesari et al., 2016). In contrast, high temperature in summer favored gas-particle partitioning in the gas phase and thus limited the formation of SOC (Strader et al., 1999). The contributions of carbonaceous components generally followed the seasonal patterns of SNA, accounting for 26.7-38.8% of $\text{PM}_{2.5}$ mass. Among these, OM showed the lowest fractions in $\text{PM}_{2.5}$ in spring (21.1%) at CD and the highest value in winter (33.6%) at CQ, while the percentages of OM in other seasons were similar at both sites, around 27%. The seasonal variations of EC fractions were not obvious, with a slightly higher value in spring.

3.1.3 Similarities and differences between the two sites

Although none of the two sites alone can represent the whole region of the Sichuan Basin, the similarities in the characteristics of the major pollutants between the two sites should represent the regional-scale characteristics of urban-environment pollution while the differences between the two sites should reflect the sub-regional characteristics of urban pollution. A comparison between the two sites in terms of seasonal-average concentrations of major chemical components is shown in Fig. 4 and discussed in detail below. Despite the 260 km distance between the two sampling sites, a moderate similarity was observed in autumn, winter and spring on the basis of low COD values (0.15-0.18), indicating limited differences between the two urban environments in the Sichuan Basin and the similarities in major emission sources for both sites. The similar pollution patterns observed at both CD and CQ were likely to be related to the similar meteorological parameters and special topography of the basin, which is a closed lowland surrounded by high mountains on all sides (Fig. 1). The mean elevation in the basin is about 200-700 m, while the surrounded mountains are around a scope of 1000-3000 m elevation. The Tibetan Plateau lies close to the western Sichuan Basin, with an elevation above 4000 m. Such a Plateau-Basin topography forms a barrier for the dispersion of pollutants and causes air stagnation within the basin, thereby facilitating regional scale pollution events in the basin. 72-h air mass back trajectory analysis (18:00 local time) showed that air masses reaching at CD and CQ mainly originated from local areas in the basin (Fig. S1), confirming the influence of the high mountainous surrounding the basin. These results were consistent with those found in earlier studies in Chengdu and Chongqing (Tian et al., 2017; Liao et al.,

254 2017), which suggested that air masses had short-range trajectories and primarily originated from inside
255 the Sichuan Basin, highlighting the impacts of the special topography on PM_{2.5} pollution. A similar case
256 has also been found elsewhere, such as in Po Valley, Italy (Ricciardelli et al., 2017).

257 It is worth to note that the COD values used to identify the similarities or differences of the two
258 sites were calculated based on seasonal-average concentrations of all the components in PM_{2.5}.
259 However, if focusing on individual components, several chemical species in PM_{2.5} differed by up to a
260 factor of 2.5 in their season-average concentrations between CD and CQ, e.g. OC and EC in winter and
261 spring, and Cl⁻ and FS in all the four seasons. In summer, the differences for several major chemical
262 components (FS, OC, SO₄²⁻, NO₃⁻ and EC) between the two sites were larger than in the other seasons,
263 causing a high COD value (0.33). These discrepancies were partly caused by the different atmospheric
264 chemical processes, local sources and meteorological parameters between the two sites. Specifically, FS
265 mostly deviated from the 1:1 straight line in all the seasons, with substantially higher concentrations at
266 CQ than CD (Fig. 4). There was no significant difference in NH₄⁺ concentrations between CD and CQ,
267 but considerable differences in SO₄²⁻ and NO₃⁻ in spring and summer. SO₂ concentration was around
268 25% higher at CQ than CD in spring and summer, which partially explained the site-differences in SO₄²⁻.
269 In contrast, NO₂ concentration was comparable at both sites in summer, but NO₃⁻ concentration was
270 58% lower in CQ than CD. The site-differences in NO₃⁻ concentration was caused by NH₄NO₃
271 thermodynamic equilibrium controlled by ambient temperature and RH, instead of by its gaseous
272 precursors. The equilibrium would be shifted toward the particulate phase when ambient RH was above
273 the deliquescence relative humidity (DRH) of NH₄NO₃, and the dissociation constant decreased by
274 about one order of magnitude when RH was above 75% (Kuprov et al., 2014). DRH was calculated
275 from temperature following Mozurkewich (1993). As shown in Table 1, the average temperature was
276 comparable at CD and CQ during the summer period, hence leading to similar DRH values of NH₄NO₃,
277 ranging from 59% to 64% with an average value of 60.7%. However, the ambient RH was substantially
278 lower at CQ (61%) than CD (72%), causing lower NO₃⁻ concentration at CQ. As shown in Fig. S2, 53%
279 of the hourly data in summer having ambient RH lower than DRH at CQ, while only 19% such data at
280 CD, which explained the different NO₃⁻ concentrations between CD and CQ.

281 Fig.4 shows higher concentrations of carbonaceous component (OC and EC) at CQ than CD in all
282 the seasons except OC in autumn and EC in winter. OC and EC mainly originate from fossil fuel
283 combustion and biomass burning. K⁺ is usually regarded as a tracer of biomass burning (Tao et al.,

2016). During the sampling campaign, no significant differences in K^+ levels were observed between CD and CQ (Table 1), suggesting that biomass burning was not be the major cause of the higher concentrations of carbonaceous component at CQ. Motorcycle traffic was likely a major source of volatile organic compounds (VOCs) in CQ since it is a famous mountain city where most people use motorcycle as daily traffic tools. The number of motorcycles was 2.0 million in Chongqing in 2014, which was much higher than those (0.7 million) in Chengdu (Chongqing and Chengdu Statistical Yearbook 2015). Moreover, Chongqing has become China's largest automobile production base, which likely also emit VOCs from the spraying process. Higher concentrations of VOCs in CQ would cause higher concentrations of secondary organic carbon via photochemical reaction under high temperature or vapor condensation under low temperature. This hypothesis is supported by the large differences in OC concentrations in winter between the two sites.

Correlation analysis may also provide an insight into the similarities/differences between the two sites over an intensive sampling period. Good correlations between the two sites were found for daily SNA, OC, EC and K^+ concentrations in autumn, winter and spring (Table S1). However, for NO_3^- , a significant correlation was identified only in autumn, likely due to the strong impact of local vehicle emissions and the subsequent atmospheric processes forming NO_3^- . Similarly, a moderate correlation was observed just in winter for both Cl^- and FS. In summer, weak or no correlations were identified between the two sites for almost all chemical components.

3.2 $PM_{2.5}$ formation mechanisms and geographical origins

3.2.1 Pollution episodes and key chemical components

Pollution episodes during the campaign are highlighted with shaded areas in Fig. 5. These pollution periods (PP) were defined as daily $PM_{2.5}$ concentration being above the NAAQS guideline value of $75 \mu g m^{-3}$. Similarly, the days with $PM_{2.5}$ concentration below $75 \mu g m^{-3}$ were characterized to be clean periods (CP). A total of seven pollution episodes were identified during the campaign at each site. There were three long-lasting pollution episodes occurred simultaneously at the two sites on 23-27 October 2014, 7(8)-26 January, and 26-28 (29) April 2015. A total of 34 and 31 pollution days were counted at CD and CQ site, respectively, accounting for 30.4% and 28.6% of the entire sampling days (112 days). The number of pollution days at CD was 8, 21, 4 and 1 in autumn, winter, spring and summer, accounting for 29.6%, 75%, 14.3% and 3.4% of the total sampling days in each season, respectively, and at CQ they were 4, 19, 6 and 2, accounting for 14.8%, 67.9%, 21.4% and 6.9%. Stagnant

314 atmosphere and high RH were important factors causing PM_{2.5} pollution events, as was found in this
315 and earlier studies (Zheng et al., 2015b;Chen et al., 2017;Liao et al., 2017). Compared with the clean
316 periods, the pollution periods were usually characterized by low planetary boundary layer height and
317 weak wind speed (Table S2), which suppressed pollutants dispersion vertically and horizontally.
318 Temperature increased during the long-lasting pollution episodes, which promoted gas-to-particle
319 transformation, forming secondary aerosols. RH remained high (68-88%) during pollution episodes
320 (except in spring at CQ), although not much different from clean periods, which was also conducive for
321 aqueous-phase reactions converting gaseous pollutants into aerosols (Chen et al., 2017;Tian et al.,
322 2017).

323 Looking more closely at a regional-scale long-lasting pollution episode in winter, from 8 January to
324 26 January 2015, the concentrations of PM_{2.5} and major chemical components increased dramatically
325 compared with clean periods (Fig. 6). PM_{2.5} concentrations were more than three times higher at both
326 sites, with the two dominant groups of components, SNA and OC, being 2.5-2.8 times higher at CD and
327 1.7-2.7 times higher at CQ. The enhancement of SNA and OC during pollution periods were similar at
328 CD, but OC increased much more than SNA at CQ, indicating some different contributing factors to the
329 high PM_{2.5} pollution at the two sites. Pollutants accumulation under stagnant meteorological conditions
330 might be a main factor at CD based on the similar magnitudes of the enhancements of PM_{2.5} and its
331 dominant components, while additional processes should have increased OC more than other
332 components at CQ. The percentage contributions of SNA to PM_{2.5} were similar during clean and
333 pollution periods, 38-41% at CD and CQ (Fig. S3). However, the percentage contributions of OM to
334 PM_{2.5} decreased from 30.1% on clean days to 27.5% on pollution days at CD, and increased from
335 26.9% to 34.9% at CQ. Concentrations of the individual SNA species (SO₄²⁻, NO₃⁻ and NH₄⁺) increased
336 by a factor of 2.5-3.3 on pollution days compared with clean days in all the cases (Fig. 6). But the
337 percentage contributions differed among the species as NO₃⁻ increased and SO₄²⁻ decreased on pollution
338 days. The percentage contributions of SNA and OM to PM_{2.5} discussed above were different from those
339 found in eastern coastal China and North China Plain, where considerable increases were found for
340 SNA and decreases for OM on pollution days than clean days (Tan et al., 2009;Wang et al., 2015a;Quan
341 et al., 2014;Zhang et al., 2015;Zhang et al., 2016;Cheng et al., 2015). The pollution periods in eastern
342 coastal China and North China Plain were accompanied with sharp increases of RH, which would
343 promote aqueous-phase formation of secondary inorganic aerosols and resulted in rapid elevation of

SO₄²⁻ and NO₃⁻ concentrations (Zheng et al., 2015b;Zheng et al., 2015a;Zhao et al., 2013b;Li et al., 2017a). In contrast, RH remained high during both clean or pollution periods in the present study, suggesting that high RH might not be the primary cause of the dramatic increase in PM_{2.5} concentrations during the pollution period in the Sichuan Basin. Another point that need to be mentioned is that, as shown in Fig. S1, local sources were the main contributors to the pollution episodes in the Sichuan Basin while sources outside local regions frequently contributed to pollution episodes in eastern coastal China and North China Plain through long/medium range transport (Gao et al., 2015;Hua et al., 2015;Wang et al., 2015b).

3.2.2 Transformation mechanisms of secondary aerosols

In most cases, meteorological conditions, atmospheric chemical processes and long-range transport are all responsible for PM_{2.5} accumulation (Zheng et al., 2015b). CO is directly emitted from combustion processes and is not very reactive. Its concentrations in the air are strongly controlled by meteorological parameters within a relatively short period, which make it a good tracer that can be used for separating different dominant factors contributing to pollutants accumulation (Zheng et al., 2015b;Zhang et al., 2015;Hu et al., 2013;Liggio et al., 2016). The impact of atmospheric physical processes on other pollutants can be revealed by scaling the concentrations of other pollutants to that of CO. For example, PM_{2.5} was enhanced by a factor of 2.7 on pollution days at both sites, but the CO-scaled PM_{2.5} (the ratio of PM_{2.5} to CO concentration) only showed an enhancement of a factor of 1.6-1.8 (Fig. 7), and the latter values were likely from the enhanced secondary aerosol formation.

As shown in Fig. 7, the CO-scaled SNA was 60-90% higher on pollution days with individual species 40-120% higher, even though their gaseous precursor (SO₂ and NO₂, no data for NH₃) were only less than 30% higher. This suggested stronger chemical transformation from gaseous precursors to particle formation on pollution days. Sulfur oxidation ratio ($SOR = n\text{-SO}_4^{2-}/(n\text{-SO}_4^{2-}+n\text{-SO}_2)$) and nitrogen oxidation ratio ($NOR = n\text{-NO}_3^-(n\text{-NO}_3^-+n\text{-NO}_2)$) were defined to evaluate the degree of secondary transformation (n refers to as the molar concentration) (Hu et al., 2014). NOR increased from 0.09 on clean days to 0.16 on pollution days at CD and from 0.07 to 0.14 at CQ. SOR increased only slightly, from 0.31 to 0.35 at CD and 0.28 to 0.35 at CQ. The CO-scaled SOC increased by a factor of 2.6 on pollution days at CQ, but no significant change was found at CD. The different patterns in SOC (or SOC/OC) than SNA (or SOR and NOR) suggested that secondary organic aerosols (SOA) production was of less important than SNA production at CD.

SO_4^{2-} is predominantly formed via homogeneous gas-phase oxidation. In this pathway, SO_2 is firstly oxidized by OH radical to SO_3 , and then to H_2SO_4 (Stockwell and Calvert, 1983;Blitz et al., 2003). Apart from homogeneous reaction, particulate SO_4^{2-} can also be formed through heterogeneous reactions with dissolved O_3 or H_2O_2 under the catalysis of transition metal and in-cloud process (Ianniello et al., 2011). HNO_3 is primarily produced from the reactions between NO_2 and OH radical during the daytime and later combines with NH_3 to produce particulate NO_3^- (Calvert and Stockwell, 1983). Particulate NO_3^- can also be formed through heterogeneous hydrolysis of N_2O_5 on moist and acidic aerosols during nighttime (Ravishankara, 1997;Brown and Stutz, 2012). Similarly, SOA is mainly formed through photochemical oxidation of primary VOCs followed by condensation of SVOC onto particles as well as through aqueous-phase reactions (Ervens et al., 2011). While photochemical reactions are mostly influenced by temperature and oxidants amount, heterogeneous reactions always depend on ambient RH. To further explore the formation mechanisms of secondary aerosols, SOR, NOR and SOC/OC data were grouped with temperature (at 2°C interval), RH (at 5% interval) and daytime O_3 concentration (at $5\text{ }\mu\text{g m}^{-3}$ interval) bins (Fig. 8). An obvious increase of SOR with increasing RH was found at both sites, but this was not the case for temperature and O_3 concentration, suggesting heterogeneous processes played important roles in the formation of SO_4^{2-} , as was suggested in many previous studies (Quan et al., 2015;Zheng et al., 2015a;Zhao et al., 2013b). Interestingly, SOR exhibited a decreasing trend with increasing O_3 concentration at O_3 concentrations lower than $15\text{ }\mu\text{g m}^{-3}$ and an opposite trend was found at O_3 concentrations above $20\text{ }\mu\text{g m}^{-3}$ (Fig. 8). Additionally, high $\text{PM}_{2.5}$ concentrations were mostly associated with lower O_3 concentrations. This behavior might be explained by the complicated interactions between aerosol and O_3 . On one hand, aerosols are generally considered as a constraining factor to O_3 production due to their absorption and scattering of UV radiation, which reduce solar radiation and consequently decrease photochemical activity. On the other hand, aerosols can provide an interface for the heterogeneous reaction, in accordance with O_3 consumption and secondary aerosol formation, which would result in decreased O_3 concentrations and increased secondary aerosols (Zheng et al., 2015b). It was further found that the ambient RH remained high at low O_3 concentrations (Fig. S4), which was beneficial to SO_4^{2-} formation through heterogeneous aqueous processes, consistent with the observed results that high SOR value occurred at low O_3 concentrations.

Unlike SOR, NOR increased with both temperature and RH, suggesting the combined effects from homogeneous and heterogeneous reactions. However, under the very high temperature and RH

404 conditions, NOR exhibited a decreasing trend with increasing temperature and RH. Volatilization of
 405 NH_4NO_3 at high temperature should be the major cause of such a phenomenon, but it is not clear about
 406 the cause of the decreasing trend of NOR under high RH. Pathak et al. (2009) investigated the formation
 407 mechanism of NO_3^- in ammonium-rich and ammonium-poor samples, suggesting homogeneous gas-
 408 phase reaction became evident to form NO_3^- under the former condition while heterogeneous process
 409 dominated the NO_3^- formation under the latter condition. As shown in Fig. 9, SO_4^{2-} and NO_3^- were
 410 almost completely neutralized by NH_4^+ , indicating an ammonium-rich environment during the sampling
 411 campaign. The ammonium-rich environment was also confirmed by the molar ratios of $[\text{NO}_3^-]/[\text{SO}_4^{2-}]$
 412 and $[\text{NH}_4^+]/[\text{SO}_4^{2-}]$. The molar ratio $[\text{NO}_3^-]/[\text{SO}_4^{2-}]$ as a function of $[\text{NH}_4^+]/[\text{SO}_4^{2-}]$ is depicted in Fig. 9,
 413 which shows significant positive correlations ($R^2=0.82-0.83$ at the two sites). Linear regression
 414 equations were obtained as $[\text{NO}_3^-]/[\text{SO}_4^{2-}] = 0.85[\text{NH}_4^+]/[\text{SO}_4^{2-}] - 1.89$ at CD and $[\text{NO}_3^-]/[\text{SO}_4^{2-}] =$
 415 $0.92[\text{NH}_4^+]/[\text{SO}_4^{2-}] - 1.82$ at CQ. Based on these equations, the molar ratio of $[\text{NH}_4^+]/[\text{SO}_4^{2-}]$ was defined
 416 as the threshold value separating ammonium-rich and ammonium-poor conditions when the value of
 417 $[\text{NO}_3^-]/[\text{SO}_4^{2-}]$ was zero. In the present study, the threshold value was 2.2 and 2.0 at CD and CQ,
 418 respectively. The molar ratio $[\text{NH}_4^+]/[\text{SO}_4^{2-}]$ was higher than the threshold value at both sites,
 419 suggesting the prevalence of ammonium-rich condition. The near-perfect fitting between the molar
 420 ratios of $[\text{NO}_3^-]/[\text{SO}_4^{2-}]$ and $[\text{NH}_4^+]/[\text{SO}_4^{2-}]$ further demonstrated the characteristics of NO_3^- formed
 421 through homogenous gas-phase reaction. Moreover, NO_3^- showed a strong correlation with excess NH_4^+
 422 with correlation coefficients of 0.98-0.99 at both sites, providing an insight into the gas-phase reactions
 423 of ambient NH_3 and HNO_3 . Using high-resolution inorganic ions data, Tian et al. (2017) demonstrated
 424 that NO_3^- was primarily formed via homogeneous reaction when RH below 75% and through
 425 heterogeneous processes when RH was above 75%. The increases in NOR with RH at both sites also
 426 revealed the possibility of the heterogeneous processes, although this cannot be verified directly due to
 427 the lack of high-resolution data.

428 The ratio of SOC/OC decreased with increasing temperature at CD but increased at CQ when
 429 temperature was lower than 10°C. Although SOC/OC did not correlate well with RH, an opposite trend
 430 was also found between CD and CQ at high RH conditions. Heterogeneous reactions seemed to be
 431 dominant in the formation of SOA at CD, whereas homogeneous reactions were prevalent at CQ.
 432 SOC/OC showed no apparent dependency on O_3 concentrations at either site, indicating more complex
 433 formation mechanisms of SOA than SO_4^{2-} and NO_3^- .

3.2.3 Geographical origins of high PM_{2.5} pollution

PSCF analysis was applied to investigate the potential source regions contributing to high PM_{2.5} pollution. As can be seen from the PSCF maps in Fig. 10, all the pollutants including PM_{2.5} and its chemical components as well as gaseous precursors had similar spatial patterns of potential source areas. Basically, all the major source areas for high pollutants concentrations were distributed within the basin. Long-range transports as seen in North Plain and eastern coastal regions were not observed at CD and CQ (Zhao et al., 2015; Zhang et al., 2013). At CD, the major source areas in winter included the areas of the northeastern, southeastern and southern Chengdu and in some areas of eastern Chongqing. A similar spatial distribution of PM_{2.5} potential sources was also found by Liao et al. (2017) through PSCF analysis in winter 2013, in which high PM_{2.5} concentrations were mostly associated with sources broadly located in the southeast of the basin, covering Neijiang, Zigong, Yibin, Luzhou and east part of Chongqing. At CQ, the northeast area of Chongqing was identified as strong sources, where a number of industries were located, such as Changshou chemical industrial ozone. Overall, PM_{2.5} pollution at CQ was characterized by significant local contribution from major sources located in or nearby Chongqing. In contrast, regional transport in Sichuan Basin from southeast, south and southwest of Chengdu had a major impact on PM_{2.5} pollution at CD.

4 Conclusions

Chemically-resolved PM_{2.5} data collected during four seasons at two urban sites in Sichuan basin, southwest China were analyzed in the present study. On about 30% of the days, daily PM_{2.5} exceeded the national air quality standard, with annual mean concentrations of 67.0 ± 43.4 and $70.9 \pm 41.4 \mu\text{g m}^{-3}$ at CD and CQ, respectively. SO_4^{2-} , NO_3^- , NH_4^+ , OM, EC and FS were the major chemical components of PM_{2.5}, accounting for 16.8%, 13.6%, 10.8%, 26.1%, 5.4%, and 5.7% of PM_{2.5} at CD, and 17.2%, 10.9%, 9.2%, 29.6%, 6.4%, and 9.5% at CQ, on annual average, respectively. The concurrent occurrences of heavy pollution events at the two sites and similarities in pollutants characteristics between the two sites was mainly caused by the surrounding mountainous topography under typical stagnant meteorological conditions. Such a finding was also supported by back trajectory analysis which showed that air masses reaching at both sites were originated within the basin and only traveled for short distances on heavy polluted days. Differences between the two sites with regards to several major chemical components provided evidences of sub-regional characteristics of emission sources and chemical transformation processes under different meteorological conditions. For example, an additional source factor from

motorcycle traffic was identified for VOCs emission in Chongqing, which led to higher OC concentrations, and lower relative humidity in Chongqing caused lower NO_3^- concentration in this city despite similar levels of its gaseous precursors in the two cities. The present study also identified different driving mechanisms for the $\text{PM}_{2.5}$ pollution episodes in the Sichuan Basin than in the other regions of China. For example, sharply increased relative humidity was thought to be one of the main factors causing high inorganic aerosol concentrations during the pollution periods in eastern coastal China and North China Plain, while in the Sichuan Basin the special topography and meteorological conditions are driving forces for such events considering relative humidity was high throughout the year and did not differ much between pollution and clean periods. However, on annual basis heterogeneous reactions might be more important in this basin than in the other regions of China due to the consistent high humidity conditions, as revealed in the case of SO_4^{2-} formation in the present study. Future studies should use high-resolution data to verify the findings related to chemical transformation paths proposed here. More importantly, a detailed emission inventory of aerosol particles and related gaseous precursors in the basin should be developed promptly, which is needed for further investigating $\text{PM}_{2.5}$ formation mechanisms and for making future emission control policies. Source-receptor analysis using monitored chemical-resolved $\text{PM}_{2.5}$ data should be conducted to verify such emission inventories.

480

Competing interests. The authors declare that they have no conflict of interest.

482

Acknowledgements. This work was supported by the National Natural Science Foundation of China (No. 41405027, 41375123, and 41403089), the "Strategic Priority Research Program" of the Chinese Academy of Sciences (No. KJZD-EW-TZ-G06), the West Action Plan of the Chinese Academy of Science (No. KZCX2-XB3-14), and Chongqing Science and Technology Commission (No. cstc2014yykfc20003, cstckjcxljrc13). We are grateful to Yumeng Zhu and Jun Wang for sample collection.

488 Reference

- Anderson, G. B., Krall, J. R., Peng, R. D., and Bell, M. L.: Is the Relation Between Ozone and Mortality Confounded by Chemical Components of Particulate Matter? Analysis of 7 Components in 57 US Communities, *Am J Epidemiol*, 176, 726-732, 10.1093/aje/kws188, 2012.
- Ashbaugh, L. L., Malm, W. C., and Sadeh, W. Z.: A Residence Time Probability Analysis of Sulfur Concentrations at Grand-Canyon-National-Park, *Atmos Environ*, 19, 1263-1270, Doi 10.1016/0004-6981(85)90256-2, 1985.
- Baumer, D., Vogel, B., Versick, S., Rinke, R., Mohler, O., and Schnaiter, M.: Relationship of visibility, aerosol optical thickness and aerosol size distribution in an ageing air mass over South-West Germany, *Atmos Environ*, 42, 989-998, 10.1016/j.atmosenv.2007.10.017, 2008.

Blitz, M. A., Hughes, K. J., and Pilling, M. J.: Determination of the high-pressure limiting rate coefficient and the enthalpy of reaction for OH+SO₂, *J Phys Chem A*, 107, 1971-1978, 10.1021/jp026524y, 2003.

Brown, S. S., and Stutz, J.: Nighttime radical observations and chemistry, *Chem Soc Rev*, 41, 6405-6447, 10.1039/c2cs35181a, 2012.

Calvert, J. G., and Stockwell, W. R.: Acid Generation in the Troposphere by Gas-Phase Chemistry, *Environ Sci Technol*, 17, A428-A443, DOI 10.1021/es00115a002, 1983.

Cao, J. J., Wang, Q. Y., Chow, J. C., Watson, J. G., Tie, X. X., Shen, Z. X., Wang, P., and An, Z. S.: Impacts of aerosol compositions on visibility impairment in Xi'an, China, *Atmos Environ*, 59, 559-566, 10.1016/j.atmosenv.2012.05.036, 2012.

Castro, L. M., Pio, C. A., Harrison, R. M., and Smith, D. J. T.: Carbonaceous aerosol in urban and rural European atmospheres: estimation of secondary organic carbon concentrations, *Atmos Environ*, 33, 2771-2781, Doi 10.1016/S1352-2310(98)00331-8, 1999.

Cesari, D., Donato, A., Conte, M., Merico, E., Giangreco, A., Giangreco, F., and Contini, D.: An inter-comparison of PM_{2.5} at urban and urban background sites: Chemical characterization and source apportionment, *Atmos Res*, 174, 106-119, 10.1016/j.atmosres.2016.02.004, 2016.

Chen, Y., and Xie, S. D.: Long-term trends and characteristics of visibility in two megacities in southwest China: Chengdu and Chongqing, *J Air Waste Manage*, 63, 1058-1069, 10.1080/10962247.2013.791348, 2013.

Chen, Y., Luo, B., and Xie, S. D.: Characteristics of the long-range transport dust events in Chengdu, Southwest China, *Atmos Environ*, 122, 713-722, 10.1016/j.atmosenv.2015.10.045, 2015.

Chen, Y., Xie, S. D., Luo, B., and Zhai, C. Z.: Particulate pollution in urban Chongqing of southwest China: Historical trends of variation, chemical characteristics and source apportionment, *Sci Total Environ*, 584, 523-534, 10.1016/j.scitotenv.2017.01.060, 2017.

Cheng, Y., He, K. B., Du, Z. Y., Zheng, M., Duan, F. K., and Ma, Y. L.: Humidity plays an important role in the PM_{2.5} pollution in Beijing, *Environ Pollut*, 197, 68-75, 10.1016/j.envpol.2014.11.028, 2015.

Chow, J. C., Watson, J. G., Chen, L. W. A., Chang, M. C. O., Robinson, N. F., Trimble, D., and Kohl, S.: The IMPROVE-A temperature protocol for thermal/optical carbon analysis: maintaining consistency with a long-term database, *J Air Waste Manage*, 57, 1014-1023, 10.3155/1047-3289.57.9.1014, 2007.

Ding, X., Wang, X. M., Gao, B., Fu, X. X., He, Q. F., Zhao, X. Y., Yu, J. Z., and Zheng, M.: Tracer-based estimation of secondary organic carbon in the Pearl River Delta, south China, *J Geophys Res-Atmos*, 117, ArtD05313 10.1029/2011jd016596, 2012.

Ervens, B., Turpin, B. J., and Weber, R. J.: Secondary organic aerosol formation in cloud droplets and aqueous particles (aqSOA): a review of laboratory, field and model studies, *Atmos Chem Phys*, 11, 11069-11102, 10.5194/acp-11-11069-2011, 2011.

Fu, X. X., Wang, X. M., Hu, Q. H., Li, G. H., Ding, X., Zhang, Y. L., He, Q. F., Liu, T. Y., Zhang, Z., Yu, Q. Q., Shen, R. Q., and Bi, X. H.: Changes in visibility with PM_{2.5} composition and relative humidity at a background site in the Pearl River Delta region, *J Environ Sci-China*, 40, 10-19, 10.1016/j.jes.2015.12.001, 2016.

Gao, J. J., Tian, H. Z., Cheng, K., Lu, L., Zheng, M., Wang, S. X., Hao, J. M., Wang, K., Hua, S. B., Zhu, C. Y., and Wang, Y.: The variation of chemical characteristics of PM_{2.5} and PM₁₀ and formation causes during two haze pollution events in urban Beijing, China, *Atmos Environ*, 107, 1-8, 10.1016/j.atmosenv.2015.02.022, 2015.

Guo, M. T., Cai, X. H., and Song, Y.: Characteristics of Low Wind-Speed Meteorology in China, *Acta Scientiarum Naturalium Universitatis Pekinensis*, 52, 219-226, 2016.

Hitzenberger, R., Berner, A., Giebl, H., Kromp, R., Larson, S. M., Rouc, A., Koch, A., Marischka, S., and Puxbaum, H.: Contribution of carbonaceous material to cloud condensation nuclei concentrations in European background (Mt. Sonnblick) and urban (Vienna) aerosols, *Atmos Environ*, 33, 2647-2659, Doi 10.1016/S1352-2310(98)00391-4, 1999.

Hu, G. Y., Zhang, Y. M., Sun, J. Y., Zhang, L. M., Shen, X. J., Lin, W. L., and Yang, Y.: Variability, formation and acidity of water-soluble ions in PM_{2.5} in Beijing based on the semi-continuous observations, *Atmos Res*, 145, 1-11,

10.1016/j.atmosres.2014.03.014, 2014.

Hu, W. W., Hu, M., Yuan, B., Jimenez, J. L., Tang, Q., Peng, J. F., Hu, W., Shao, M., Wang, M., Zeng, L. M., Wu, Y. S., Gong, Z. H., Huang, X. F., and He, L. Y.: Insights on organic aerosol aging and the influence of coal combustion at a regional receptor site of central eastern China, *Atmos Chem Phys*, 13, 10095-10112, 10.5194/acp-13-10095-2013, 2013.

Hua, Y., Cheng, Z., Wang, S. X., Jiang, J. K., Chen, D. R., Cai, S. Y., Fu, X., Fu, Q. Y., Chen, C. H., Xu, B. Y., and Yu, J. Q.: Characteristics and source apportionment of PM_{2.5} during a fall heavy haze episode in the Yangtze River Delta of China, *Atmos Environ*, 123, 380-391, 10.1016/j.atmosenv.2015.03.046, 2015.

Huang, X. H. H., Bian, Q. J., Ng, W. M., Louie, P. K. K., and Yu, J. Z.: Characterization of PM_{2.5} Major Components and Source Investigation in Suburban Hong Kong: A One Year Monitoring Study, *Aerosol Air Qual Res*, 14, 237-250, 10.4209/aaqr.2013.01.0020, 2014.

Ianniello, A., Spataro, F., Esposito, G., Allegrini, I., Hu, M., and Zhu, T.: Chemical characteristics of inorganic ammonium salts in PM_{2.5} in the atmosphere of Beijing (China), *Atmos Chem Phys*, 11, 10803-10822, 10.5194/acp-11-10803-2011, 2011.

Ji, D. S., Zhang, J. K., He, J., Wang, X. J., Pang, B., Liu, Z. R., Wang, L. L., and Wang, Y. S.: Characteristics of atmospheric organic and elemental carbon aerosols in urban Beijing, China, *Atmos Environ*, 125, 293-306, 10.1016/j.atmosenv.2015.11.020, 2016.

Kuprov, R., Eatough, D. J., Cruickshank, T., Olson, N., Cropper, P. M., and Hansen, J. C.: Composition and secondary formation of fine particulate matter in the Salt Lake Valley: Winter 2009, *J Air Waste Manage*, 64, 957-969, 10.1080/10962247.2014.903878, 2014.

Larssen, T., Lydersen, E., Tang, D. G., He, Y., Gao, J. X., Liu, H. Y., Duan, L., Seip, H. M., Vogt, R. D., Mulder, J., Shao, M., Wang, Y. H., Shang, H., Zhang, X. S., Solberg, S., Aas, W., Okland, T., Eilertsen, O., Angell, V., Liu, Q. R., Zhao, D. W., Xiang, R. J., Xiao, J. S., and Luo, J. H.: Acid rain in China, *Environ Sci Technol*, 40, 418-425, DOI 10.1021/es0626133, 2006.

Lepeule, J., Laden, F., Dockery, D., and Schwartz, J.: Chronic Exposure to Fine Particles and Mortality: An Extended Follow-up of the Harvard Six Cities Study from 1974 to 2009, *Environ Health Persp*, 120, 965-970, 10.1289/ehp.1104660, 2012.

Li, B., Zhang, J., Zhao, Y., Yuan, S. Y., Zhao, Q. Y., Shen, G. F., and Wu, H. S.: Seasonal variation of urban carbonaceous aerosols in a typical city Nanjing in Yangtze River Delta, China, *Atmos Environ*, 106, 223-231, 10.1016/j.atmosenv.2015.01.064, 2015.

Li, H. Y., Zhang, Q., Zhang, Q., Chen, C. R., Wang, L. T., Wei, Z., Zhou, S., Parworth, C., Zheng, B., Canonaco, F., Prevot, A. S. H., Chen, P., Zhang, H. L., Wallington, T. J., and He, K. B.: Wintertime aerosol chemistry and haze evolution in an extremely polluted city of the North China Plain: significant contribution from coal and biomass combustion, *Atmos Chem Phys*, 17, 4751-4768, 10.5194/acp-17-4751-2017, 2017a.

Li, L. L., Tan, Q. W., Zhang, Y. H., Feng, M., Qu, Y., An, J. L., and Liu, X. G.: Characteristics and source apportionment of PM_{2.5} during persistent extreme haze events in Chengdu, southwest China, *Environ Pollut*, 230, 718-729, 10.1016/j.envpol.2017.07.029, 2017b.

Liao, T. T., Wang, S., Ai, J., Gui, K., Duan, B. L., Zhao, Q., Zhang, X., Jiang, W. T., and Sun, Y.: Heavy pollution episodes, transport pathways and potential sources of PM_{2.5} during the winter of 2013 in Chengdu (China), *Sci Total Environ*, 584, 1056-1065, 10.1016/j.scitotenv.2017.01.160, 2017.

Liggio, J., Li, S. M., Hayden, K., Taha, Y. M., Stroud, C., Darlington, A., Drollette, B. D., Gordon, M., Lee, P., Liu, P., Leithead, A., Moussa, S. G., Wang, D., O'Brien, J., Mittermeier, R. L., Brook, J. R., Lu, G., Staebler, R. M., Han, Y. M., Tokarek, T. W., Osthoff, H. D., Makar, P. A., Zhang, J. H., Plata, D. L., and Gentner, D. R.: Oil sands operations as a large source of secondary organic aerosols, *Nature*, 534, 91-94, 10.1038/nature17646, 2016.

Lu, Z., Zhang, Q., and Streets, D. G.: Sulfur dioxide and primary carbonaceous aerosol emissions in China and India, 1996-2010, *Atmos Chem Phys*, 11, 9839-9864, 10.5194/acp-11-9839-2011, 2011.

Mahowald, N.: Aerosol Indirect Effect on Biogeochemical Cycles and Climate, *Science*, 334, 794-796,

10.1126/science.1207374, 2011.

Mozurkewich, M.: The Dissociation-Constant of Ammonium-Nitrate and Its Dependence on Temperature, Relative-Humidity and Particle-Size, *Atmos Environ a-Gen*, 27, 261-270, Doi 10.1016/0960-1686(93)90356-4, 1993.

Paraskevopoulou, D., Liakakou, E., Gerasopoulos, E., and Mihalopoulos, N.: Sources of atmospheric aerosol from long-term measurements (5 years) of chemical composition in Athens, Greece, *Sci Total Environ*, 527, 165-178, 10.1016/j.scitotenv.2015.04.022, 2015.

Pathak, R. K., Wu, W. S., and Wang, T.: Summertime PM_{2.5} ionic species in four major cities of China: nitrate formation in an ammonia-deficient atmosphere, *Atmos Chem Phys*, 9, 1711-1722, 2009.

Polissar, A. V., Hopke, P. K., Paatero, P., Kaufmann, Y. J., Hall, D. K., Bodhaine, B. A., Dutton, E. G., and Harris, J. M.: The aerosol at Barrow, Alaska: long-term trends and source locations, *Atmos Environ*, 33, 2441-2458, Doi 10.1016/S1352-2310(98)00423-3, 1999.

Qu, W. J., Wang, J., Zhang, X. Y., Wang, D., and Sheng, L. F.: Influence of relative humidity on aerosol composition: Impacts on light extinction and visibility impairment at two sites in coastal area of China, *Atmos Res*, 153, 500-511, 10.1016/j.atmosres.2014.10.009, 2015.

Quan, J. N., Tie, X. X., Zhang, Q., Liu, Q., Li, X., Gao, Y., and Zhao, D. L.: Characteristics of heavy aerosol pollution during the 2012-2013 winter in Beijing, China, *Atmos Environ*, 88, 83-89, 10.1016/j.atmosenv.2014.01.058, 2014.

Quan, J. N., Liu, Q., Li, X., Gao, Y., Jia, X. C., Sheng, J. J., and Liu, Y. G.: Effect of heterogeneous aqueous reactions on the secondary formation of inorganic aerosols during haze events, *Atmos Environ*, 122, 306-312, 10.1016/j.atmosenv.2015.09.068, 2015.

Ramanathan, V., and Feng, Y.: Air pollution, greenhouse gases and climate change: Global and regional perspectives, *Atmos Environ*, 43, 37-50, 10.1016/j.atmosenv.2008.09.063, 2009.

Ravishankara, A. R.: Heterogeneous and multiphase chemistry in the troposphere, *Science*, 276, 1058-1065, DOI 10.1126/science.276.5315.1058, 1997.

Ricciardelli, I., Bacco, D., Rinaldi, M., Bonafe, G., Scotto, F., Trentini, A., Bertacci, G., Ugolini, P., Zigola, C., Rovere, F., Maccone, C., Pironi, C., and Poluzzi, V.: A three-year investigation of daily PM_{2.5} main chemical components in four sites: the routine measurement program of the Supersito Project (Po Valley, Italy), *Atmos Environ*, 152, 418-430, 10.1016/j.atmosenv.2016.12.052, 2017.

Sahu, L. K., Kondo, Y., Miyazaki, Y., Pongkiatkul, P., and Oanh, N. T. K.: Seasonal and diurnal variations of black carbon and organic carbon aerosols in Bangkok, *J Geophys Res-Atmos*, 116, ArtId15302 10.1029/2010jd015563, 2011.

Squizzato, S., Masiol, M., Brunelli, A., Pistollato, S., Tarabotti, E., Rampazzo, G., and Pavoni, B.: Factors determining the formation of secondary inorganic aerosol: a case study in the Po Valley (Italy), *Atmos Chem Phys*, 13, 1927-1939, 10.5194/acp-13-1927-2013, 2013.

Squizzato, S., and Masiol, M.: Application of meteorology-based methods to determine local and external contributions to particulate matter pollution: A case study in Venice (Italy), *Atmos Environ*, 119, 69-81, 10.1016/j.atmosenv.2015.08.026, 2015.

Stockwell, W. R., and Calvert, J. G.: The Mechanism of the HO-SO₂ Reaction, *Atmos Environ*, 17, 2231-2235, Doi 10.1016/0004-6981(83)90220-2, 1983.

Strader, R., Lurmann, F., and Pandis, S. N.: Evaluation of secondary organic aerosol formation in winter, *Atmos Environ*, 33, 4849-4863, Doi 10.1016/S1352-2310(99)00310-6, 1999.

Tan, J. H., Duan, J. C., He, K. B., Ma, Y. L., Duan, F. K., Chen, Y., and Fu, J. M.: Chemical characteristics of PM_{2.5} during a typical haze episode in Guangzhou, *J Environ Sci-China*, 21, 774-781, 10.1016/S1001-0742(08)62340-2, 2009.

Tan, J. H., Duan, J. C., Ma, Y. L., He, K. B., Cheng, Y., Deng, S. X., Huang, Y. L., and Si-Tu, S. P.: Long-term trends of chemical characteristics and sources of fine particle in Foshan City, Pearl River Delta: 2008-2014, *Sci Total Environ*, 565, 519-528, 10.1016/j.scitotenv.2016.05.059, 2016.

Tao, J., Zhang, L. M., Engling, G., Zhang, R. J., Yang, Y. H., Cao, J. J., Zhu, C. S., Wang, Q. Y., and Luo, L.: Chemical composition of PM_{2.5} in an urban environment in Chengdu, China: Importance of springtime dust storms and biomass

burning, *Atmos Res*, 122, 270-283, 10.1016/j.atmosres.2012.11.004, 2013.

Tao, J., Gao, J., Zhang, L., Zhang, R., Che, H., Zhang, Z., Lin, Z., Jing, J., Cao, J., and Hsu, S. C.: PM_{2.5} pollution in a megacity of southwest China: source apportionment and implication, *Atmos Chem Phys*, 14, 8679-8699, 10.5194/acp-14-8679-2014, 2014.

Tao, J., Zhang, L. M., Zhang, R. J., Wu, Y. F., Zhang, Z. S., Zhang, X. L., Tang, Y. X., Cao, J. J., and Zhang, Y. H.: Uncertainty assessment of source attribution of PM_{2.5} and its water-soluble organic carbon content using different biomass burning tracers in positive matrix factorization analysis - a case study in Beijing, China, *Sci Total Environ*, 543, 326-335, 10.1016/j.scitotenv.2015.11.057, 2016.

Tao, J., Zhang, L. M., Cao, J. J., and Zhang, R. J.: A review of current knowledge concerning PM_{2.5} chemical composition, aerosol optical properties and their relationships across China, *Atmos Chem Phys*, 17, 9485-9518, 10.5194/acp-17-9485-2017, 2017.

Taus, N., Tarulescu, S., Idomir, M., and Taus, R.: Respiratory exposure to air pollutants, *J Environ Prot Ecol*, 9, 15-25, 2008.

Tian, M., Wang, H. B., Chen, Y., Zhang, L. M., Shi, G. M., Liu, Y., Yu, J. Y., Zhai, C. Z., Wang, J., and Yang, F. M.: Highly time-resolved characterization of water-soluble inorganic ions in PM_{2.5} in a humid and acidic mega city in Sichuan Basin, China, *Sci Total Environ*, 580, 224-234, 10.1016/j.scitotenv.2016.12.048, 2017.

Tian, Y. Z., Wu, J. H., Shi, G. L., Wu, J. Y., Zhang, Y. F., Zhou, L. D., Zhang, P., and Feng, Y. C.: Long-term variation of the levels, compositions and sources of size-resolved particulate matter in a megacity in China, *Sci Total Environ*, 463, 462-468, 10.1016/j.scitotenv.2013.06.055, 2013.

Tie, X. X., and Cao, J. J.: Aerosol pollution in China: Present and future impact on environment, *Particuology*, 7, 426-431, 10.1016/j.partic.2009.09.003, 2009.

Turpin, B. J., and Lim, H. J.: Species contributions to PM_{2.5} mass concentrations: Revisiting common assumptions for estimating organic mass, *Aerosol Sci Tech*, 35, 602-610, Doi 10.1080/02786820152051454, 2001.

Wang, D. F., Zhou, B., Fu, Q. Y., Zhao, Q. B., Zhang, Q., Chen, J. M., Yang, X., Duan, Y. S., and Li, J.: Intense secondary aerosol formation due to strong atmospheric photochemical reactions in summer: observations at a rural site in eastern Yangtze River Delta of China, *Sci Total Environ*, 571, 1454-1466, 10.1016/j.scitotenv.2016.06.212, 2016.

Wang, H. B., Shi, G. M., Tian, M., Zhang, L. M., Chen, Y., Yang, F. M., and Cao, X. Y.: Aerosol optical properties and chemical composition apportionment in Sichuan Basin, China, *Sci Total Environ*, 577, 245-257, 10.1016/j.scitotenv.2016.10.173, 2017.

Wang, H. L., Qiao, L. P., Lou, S. R., Zhou, M., Chen, J. M., Wang, Q., Tao, S. K., Chen, C. H., Huang, H. Y., Li, L., and Huang, C.: PM_{2.5} pollution episode and its contributors from 2011 to 2013 in urban Shanghai, China, *Atmos Environ*, 123, 298-305, 10.1016/j.atmosenv.2015.08.018, 2015a.

Wang, Q. Z., Zhuang, G. S., Huang, K., Liu, T. N., Deng, C. R., Xu, J., Lin, Y. F., Guo, Z. G., Chen, Y., Fu, Q. Y., Fu, J. S. S., and Chen, J. K.: Probing the severe haze pollution in three typical regions of China: Characteristics, sources and regional impacts, *Atmos Environ*, 120, 76-88, 10.1016/j.atmosenv.2015.08.076, 2015b.

Wongphatarakul, V., Friedlander, S. K., and Pinto, J. P.: A comparative study of PM_{2.5} ambient aerosol chemical databases, *Environ Sci Technol*, 32, 3926-3934, Doi 10.1021/Es9800582, 1998.

Yang, F., Huang, L., Duan, F., Zhang, W., He, K., Ma, Y., Brook, J. R., Tan, J., Zhao, Q., and Cheng, Y.: Carbonaceous species in PM_{2.5} at a pair of rural/urban sites in Beijing, 2005-2008, *Atmos Chem Phys*, 11, 7893-7903, 10.5194/acp-11-7893-2011, 2011a.

Yang, F., Tan, J., Zhao, Q., Du, Z., He, K., Ma, Y., Duan, F., Chen, G., and Zhao, Q.: Characteristics of PM_{2.5} speciation in representative megacities and across China, *Atmos Chem Phys*, 11, 5207-5219, 10.5194/acp-11-5207-2011, 2011b.

Yang, Y. R., Liu, X. G., Qu, Y., An, J. L., Jiang, R., Zhang, Y. H., Sun, Y. L., Wu, Z. J., Zhang, F., Xu, W. Q., and Ma, Q. X.: Characteristics and formation mechanism of continuous hazes in China: a case study during the autumn of 2014 in the North China Plain, *Atmos Chem Phys*, 15, 8165-8178, 10.5194/acp-15-8165-2015, 2015.

Zhang, Q., Quan, J. N., Tie, X. X., Li, X., Liu, Q., Gao, Y., and Zhao, D. L.: Effects of meteorology and secondary particle formation on visibility during heavy haze events in Beijing, China, *Sci Total Environ*, 502, 578-584,

10.1016/j.scitotenv.2014.09.079, 2015.

Zhang, R., Jing, J., Tao, J., Hsu, S. C., Wang, G., Cao, J., Lee, C. S. L., Zhu, L., Chen, Z., Zhao, Y., and Shen, Z.: Chemical characterization and source apportionment of PM_{2.5} in Beijing: seasonal perspective, *Atmos Chem Phys*, 13, 7053-7074, 10.5194/acp-13-7053-2013, 2013.

Zhang, Y., Huang, W., Cai, T. Q., Fang, D. Q., Wang, Y. Q., Song, J., Hu, M., and Zhang, Y. X.: Concentrations and chemical compositions of fine particles (PM_{2.5}) during haze and non-haze days in Beijing, *Atmos Res*, 174, 62-69, 10.1016/j.atmosres.2016.02.003, 2016.

Zhang, Y. H., Hu, M., Zhong, L. J., Wiedensohler, A., Liu, S. C., Andreae, M. O., Wang, W., and Fan, S. J.: Regional Integrated Experiments on Air Quality over Pearl River Delta 2004 (PRIDE-PRD2004): Overview, *Atmos Environ*, 42, 6157-6173, 10.1016/j.atmosenv.2008.03.025, 2008.

Zhao, M. F., Huang, Z. S., Qiao, T., Zhang, Y. K., Xiu, G. L., and Yu, J. Z.: Chemical characterization, the transport pathways and potential sources of PM_{2.5} in Shanghai: Seasonal variations, *Atmos Res*, 158, 66-78, 10.1016/j.atmosres.2015.02.003, 2015.

Zhao, P. S., Dong, F., He, D., Zhao, X. J., Zhang, X. L., Zhang, W. Z., Yao, Q., and Liu, H. Y.: Characteristics of concentrations and chemical compositions for PM_{2.5} in the region of Beijing, Tianjin, and Hebei, China, *Atmos Chem Phys*, 13, 4631-4644, 10.5194/acp-13-4631-2013, 2013a.

Zhao, X. J., Zhao, P. S., Xu, J., Meng, W., Pu, W. W., Dong, F., He, D., and Shi, Q. F.: Analysis of a winter regional haze event and its formation mechanism in the North China Plain, *Atmos Chem Phys*, 13, 5685-5696, 10.5194/acp-13-5685-2013, 2013b.

Zheng, B., Zhang, Q., Zhang, Y., He, K. B., Wang, K., Zheng, G. J., Duan, F. K., Ma, Y. L., and Kimoto, T.: Heterogeneous chemistry: a mechanism missing in current models to explain secondary inorganic aerosol formation during the January 2013 haze episode in North China, *Atmos Chem Phys*, 15, 2031-2049, 10.5194/acp-15-2031-2015, 2015a.

Zheng, G. J., Duan, F. K., Su, H., Ma, Y. L., Cheng, Y., Zheng, B., Zhang, Q., Huang, T., Kimoto, T., Chang, D., Poschl, U., Cheng, Y. F., and He, K. B.: Exploring the severe winter haze in Beijing: the impact of synoptic weather, regional transport and heterogeneous reactions, *Atmos Chem Phys*, 15, 2969-2983, 10.5194/acp-15-2969-2015, 2015b.

Table 1 Meteorological parameters, annual and seasonal mean concentrations of PM_{2.5}, gaseous pollutants and major chemical components at CD and CQ during 2014-2015.

	CD					CQ				
	Autumn	Winter	Spring	Summer	Annual	Autumn	Winter	Spring	Summer	Annual
Meteorological parameters										
T (°C)	15.8±2.9	9.3±2.5	20.4±4.4	28.3±2.9	18.5±7.7	16.0±3.2	10.0±2.3	20.5±4.5	28.4±3.4	18.8±7.6
P (hPa)	960±3.8	963±4.7	954±7.9	946±2.1	955±8.1	981±4.2	984±5.2	974±8.4	963±2.2	975±7.7
RH (%)	81.9±9.0	80.9±6.8	70.5±8.6	72.2±11.3	76.3±10.3	76.1±5.7	68.7±8.8	60.7±13.6	61.0±13.3	66.5±12.5
SR (w m ⁻²)	54.9±40.3	37.8±27.2	128.9±65.0	123.6±94.2	67.2±56.7	na.	na.	na.	na.	na.
WS (m s ⁻¹)	0.5±0.2	0.4±0.3	0.7±0.4	0.5±0.2	0.5±0.3	0.7±0.2	0.7±0.3	1.0±0.4	0.7±0.3	0.8±0.3
Precipitation (mm)	76.3	18.3	56.6	247.8	na.	73.3	22.0	104.6	206.3	na.
PBLH _{max} (m)	890±305	852±273	1296±491	1422±529	1119±481	821±252	928±260	1310±491	1329±505	1101±453
Concentrations of gaseous pollutants (µg m ⁻³)										
O ₃	19.3±10.5	11.9±7.6	69.3±22.9	90.5±33.3	48.2±39.6	13.3±8.9	12.5±7.7	56.3±23.5	42.8±17.2	31.5±24.5
SO ₂	15.8±7.0	21.5±9.5	11.2±6.3	11.3±4.7	14.9±3.7	16.4±4.6	23.3±9.2	13.9±5.3	14.4±5.4	17.0±7.3
NO ₂	60.2±18.7	75.3±24.5	51.8±26.8	54.2±9.4	60.4±22.5	66.5±15.0	81.3±19.8	50.8±16.7	51.7±20.8	62.4±22.0

Concentrations of PM_{2.5} and chemical compositions (µg m⁻³)

PM _{2.5}	62.1±38.4	113.5±47.8	48.0±25.2	45.1±15.2	67.0±43.4	56.3±23.6	115.1±53.9	58.3±24.6	54.2±16.2	70.9±41.4
SO ₄ ²⁻	10.5±6.5	16.4±7.1	8.3±5.9	9.7±4.7	11.2±6.8	9.9±4.7	17.5±7.4	10.4±6.5	11.1±5.7	12.2±6.8
NO ₃ ⁻	9.3±7.4	17.5±8.8	5.9±3.6	3.9±2.2	9.1±8.0	7.8±3.8	15.8±9.5	5.9±5.0	1.6±1.3	7.7±7.6
NH ₄ ⁺	6.9±4.8	12.7±5.4	5.1±3.2	4.2±1.9	7.2±5.2	5.7±2.8	11.3±5.2	5.2±3.0	4.0±2.1	6.6±4.4
Cl ⁻	1.9±1.2	3.4±1.9	0.6±0.4	0.2±0.2	1.5±1.7	0.8±0.4	1.6±1.2	0.5±0.5	0.04±0.03	0.7±0.9
K ⁺	0.6±0.4	1.2±0.6	0.6±0.5	0.5±0.2	0.7±0.5	0.5±0.2	1.2±0.7	0.5±0.2	0.3±0.1	0.6±0.5
OC	10.4±6.1	19.7±8.4	6.3±3.7	7.4±1.5	10.9±7.6	9.7±4.7	24.2±13.6	10.0±5.1	8.5±3.4	13.1±10.0
EC	3.0±2.1	6.3±3.0	2.7±2.3	2.5±0.7	3.6±2.7	3.8±1.7	5.9±3.2	4.7 ±3.0	3.7±1.5	4.5±2.6
FS	3.2±1.6	4.5±2.0	4.8±3.0	2.7±1.5	3.8±2.2	5.0±2.8	6.3±3.3	9.1±7.6	6.5±4.0	6.7±5.0

na. means no data.

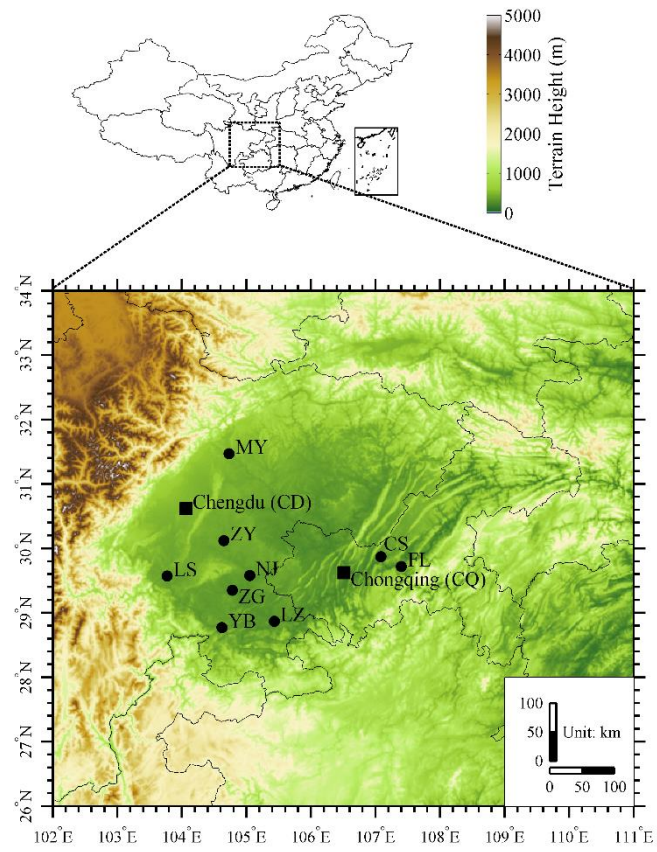


Figure 1. Locations of the sampling sites in Chengdu (CD) and Chongqing (CQ) and major cities in the Sichuan Basin. MY, Mianyang; ZY, Ziyang; LS, Leshan; NJ, Neijiang; ZG, Zigong; YB, Yibin; LZ, Luzhou; CS, Changshou; FL, Fuling.

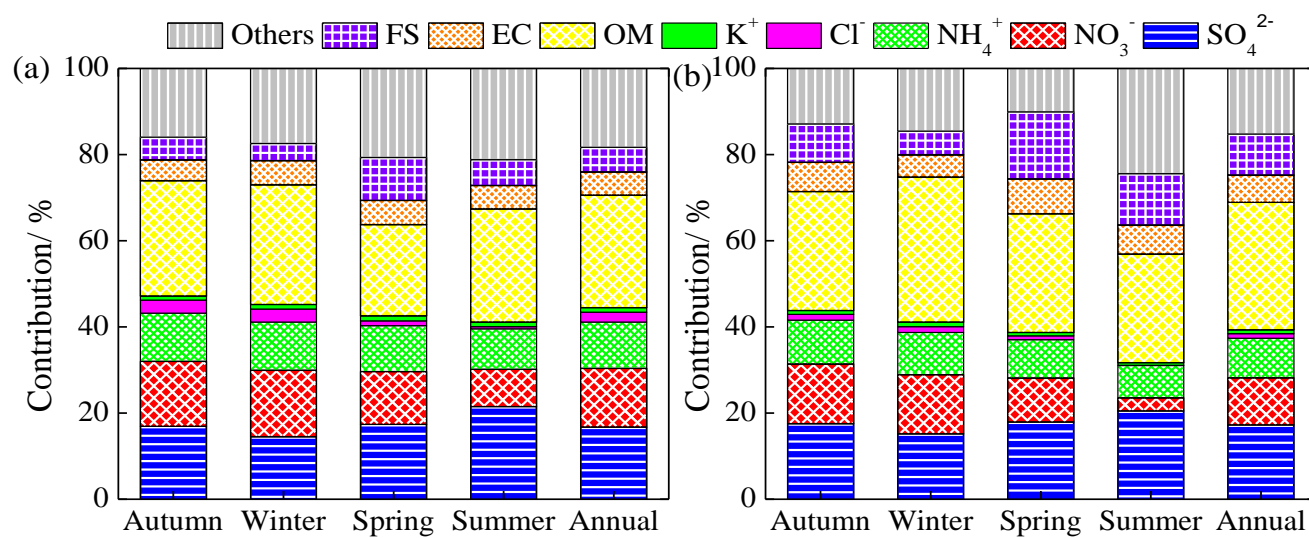


Figure 2. Seasonal and annual contributions of individual chemical components to PM_{2.5} at CD (a) and CQ (b).

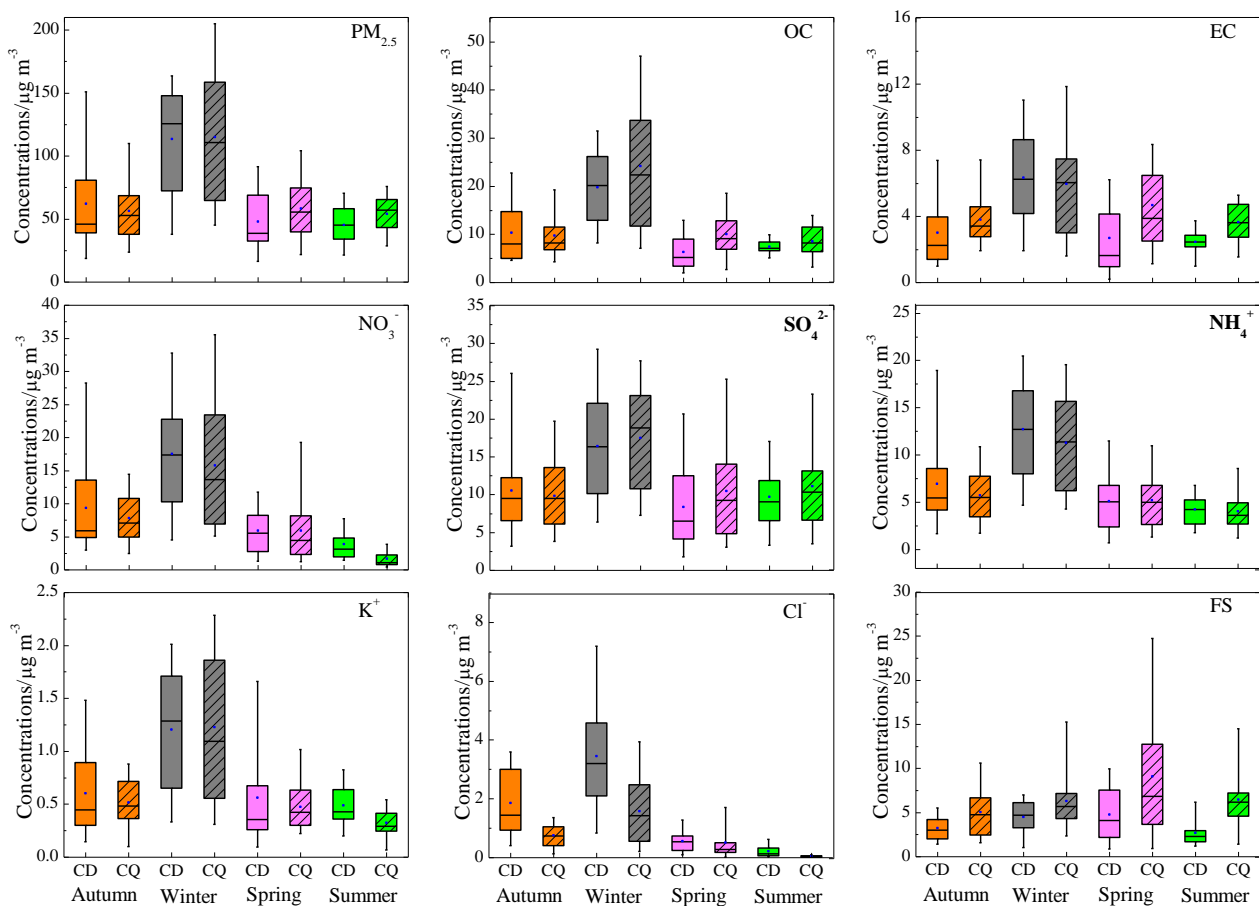


Figure 3. Seasonal distributions of PM_{2.5} and its major chemical components. Shown in each sub-figure are mean (dot symbol), median (horizontal line), the central 50% data (25th -75th percentiles, box), and the central 90% data (5th-95th percentile, whisker)

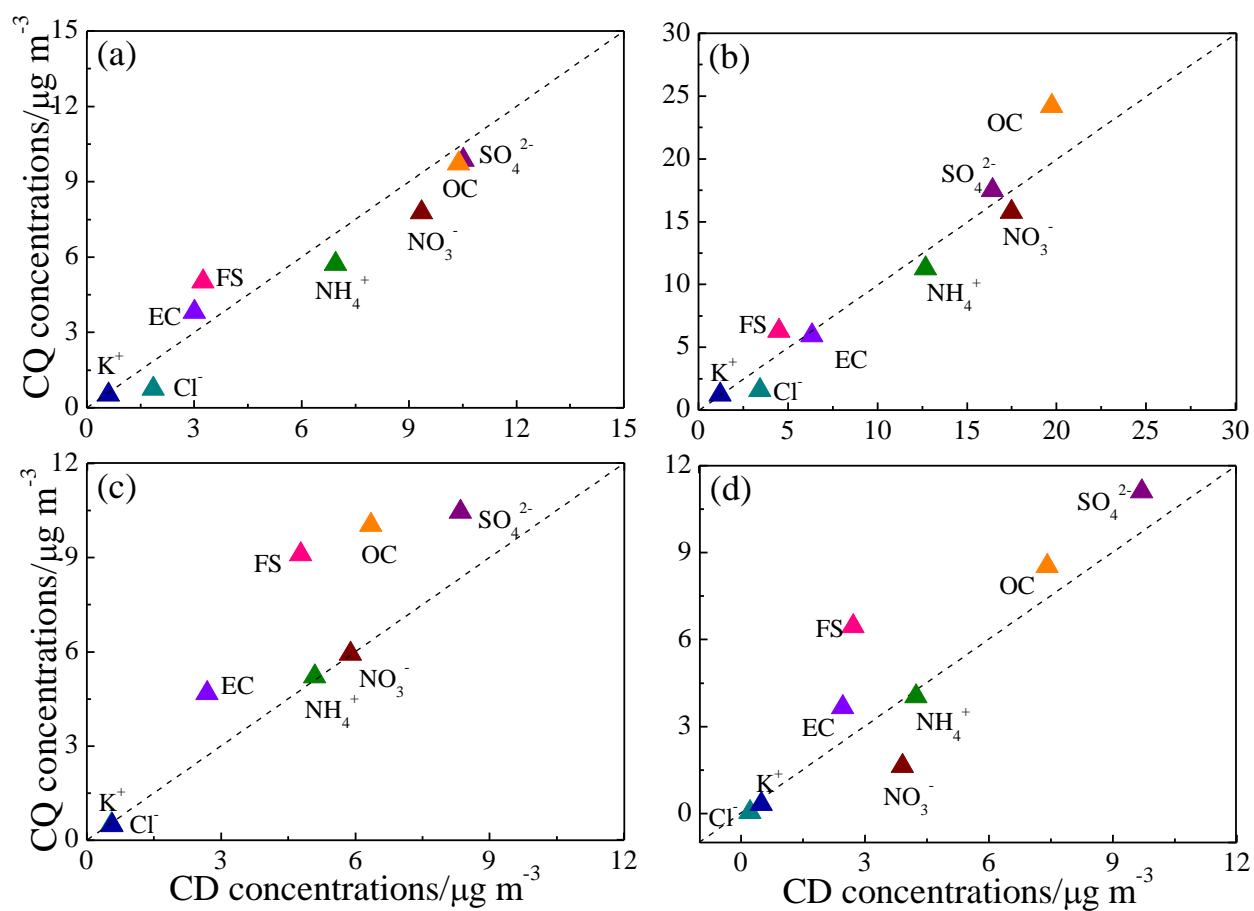


Figure 4. Seasonal mean concentrations of major components in autumn (a), winter (b), spring (c), and summer (d) at CD and CQ sites.

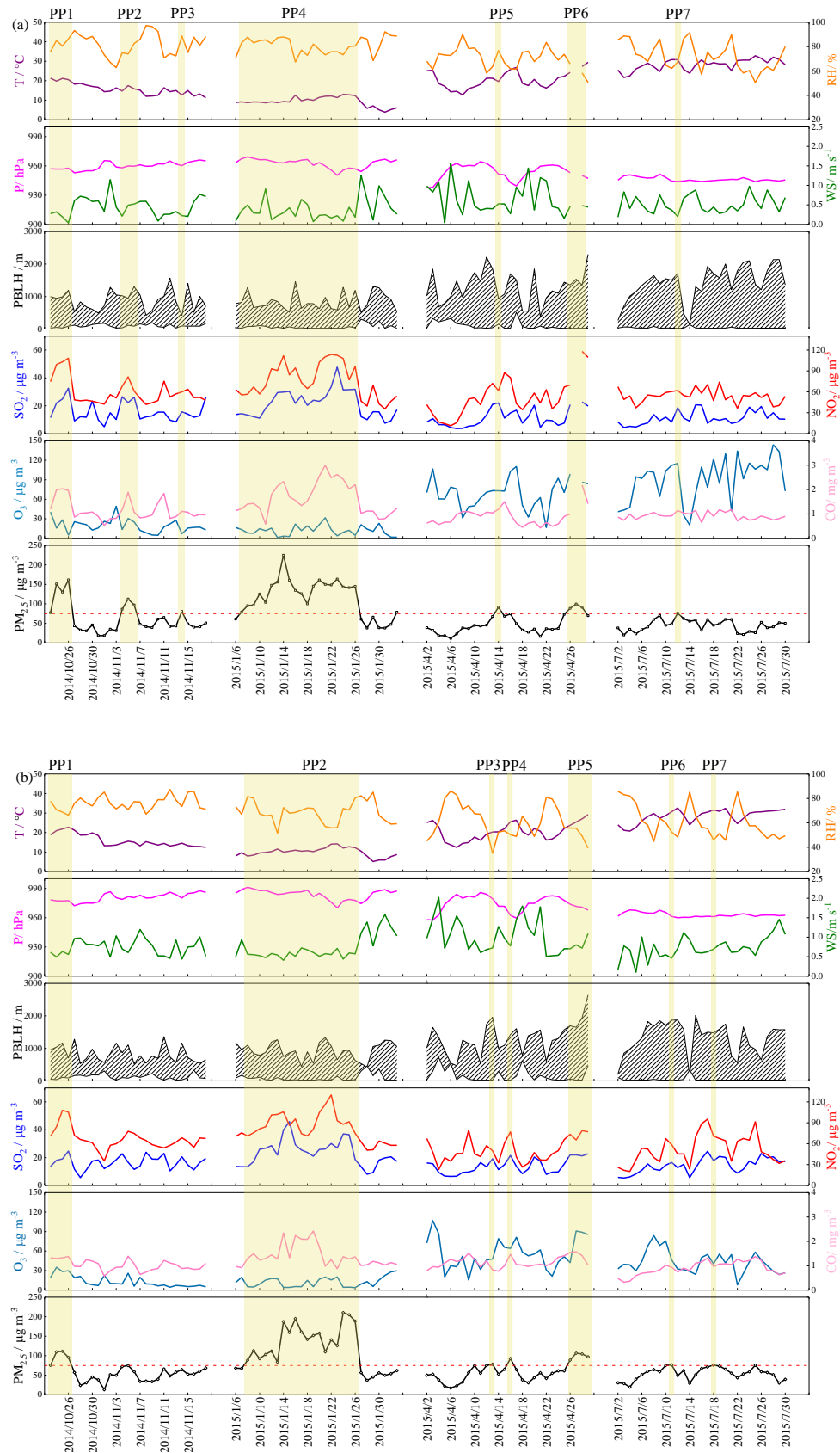


Figure 5 Temporal variations of meteorological parameters, gaseous pollutants and $\text{PM}_{2.5}$ during the campaign at CD (a) and CQ (b). Pollution episodes are highlighted by shaded areas.

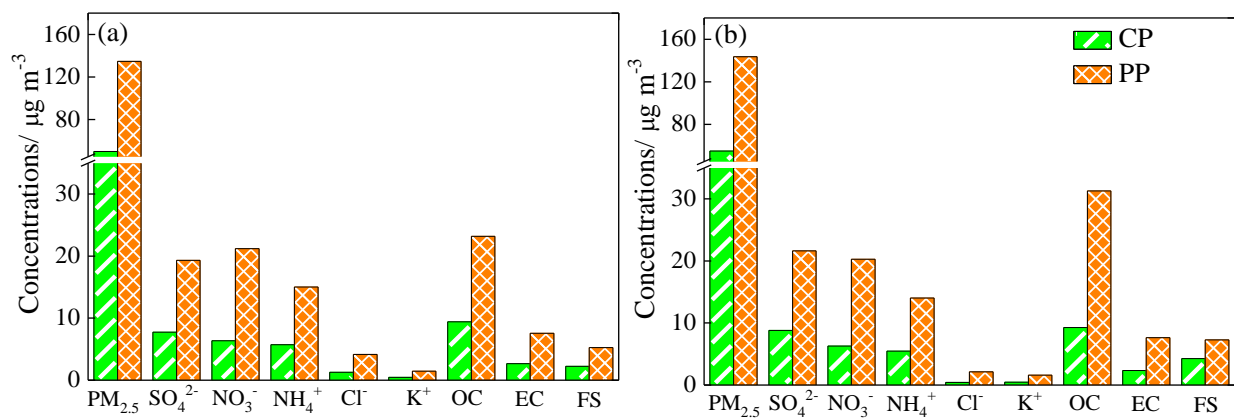


Figure 6. PM_{2.5} and major chemical components during clean periods (CP) and pollution periods (PP) in winter at CD (a) and CQ (b). At CD: CP, 6 January and 27 January-2 February 2015; PP, 7-26 January 2015. At CQ: CP, 6-7 January and 27 January-2 February 2015; PP, 8-26 January 2015.

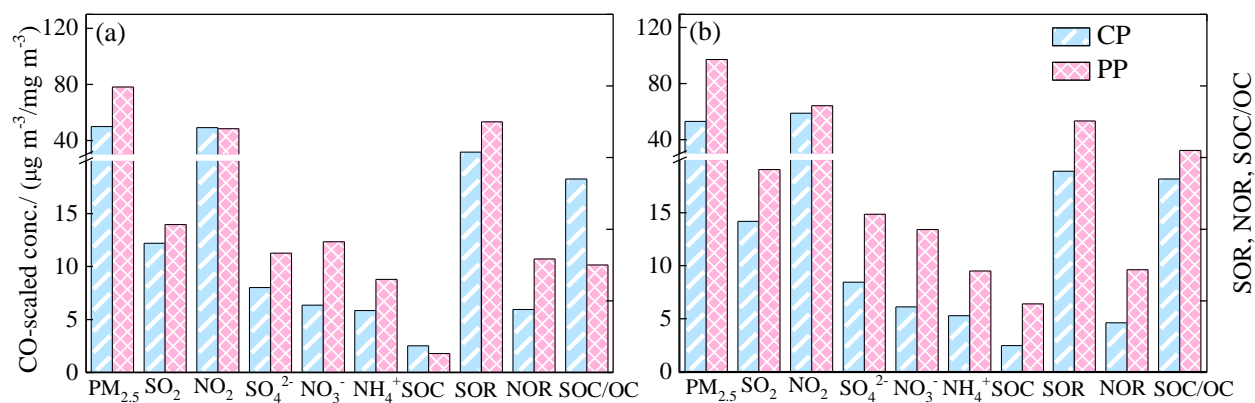


Figure 7. CO-scaled concentrations of various pollutants and the values of SOR, NOR, and SOC/OC in winter at CD (a) and CQ (b). CP and PP is the same period as Figure 6.

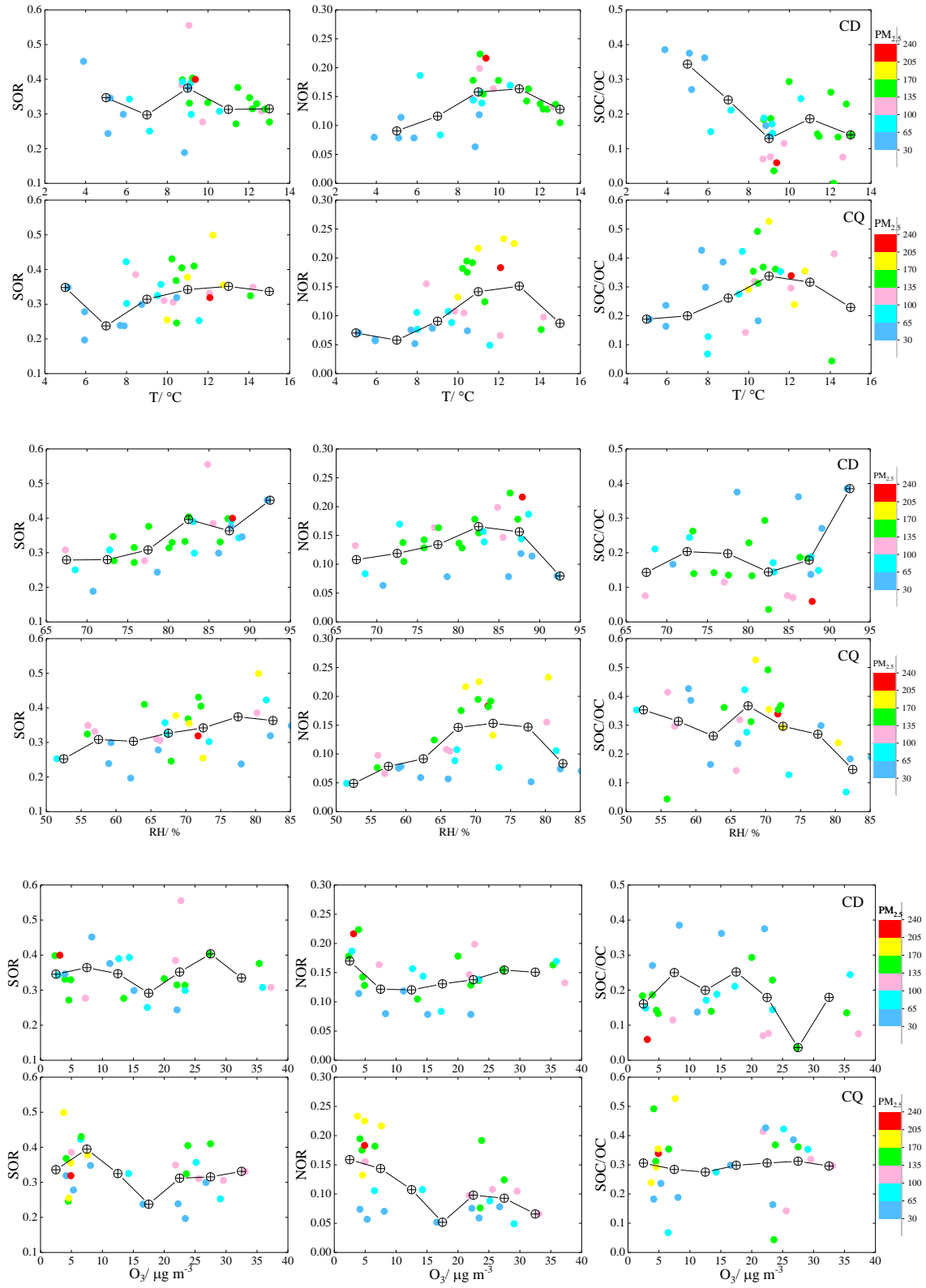


Figure 8. Correlations of SOR, NOR and SOC/OC against temperature (upper), RH (middle) and O₃ concentration (bottom) in winter at CD and CQ.

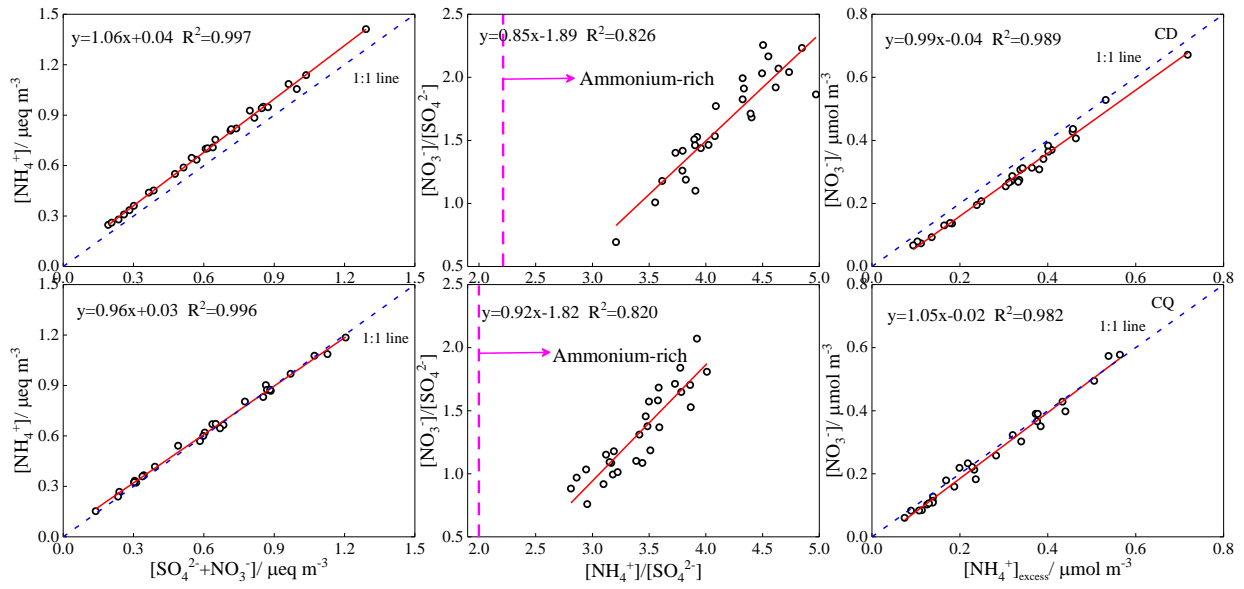


Figure 9. NH_4^+ concentration as a function of the sum of SO_4^{2-} and NO_3^- in equivalent concentrations (left column), molar ratio $\text{NO}_3^-/\text{SO}_4^{2-}$ as a function of $\text{NH}_4^+/\text{SO}_4^{2-}$ (middle column), and NO_3^- concentration as a function of $\text{NH}_4^+_{\text{excess}}$ (right column) at CD (upper row) and CQ (lower row).

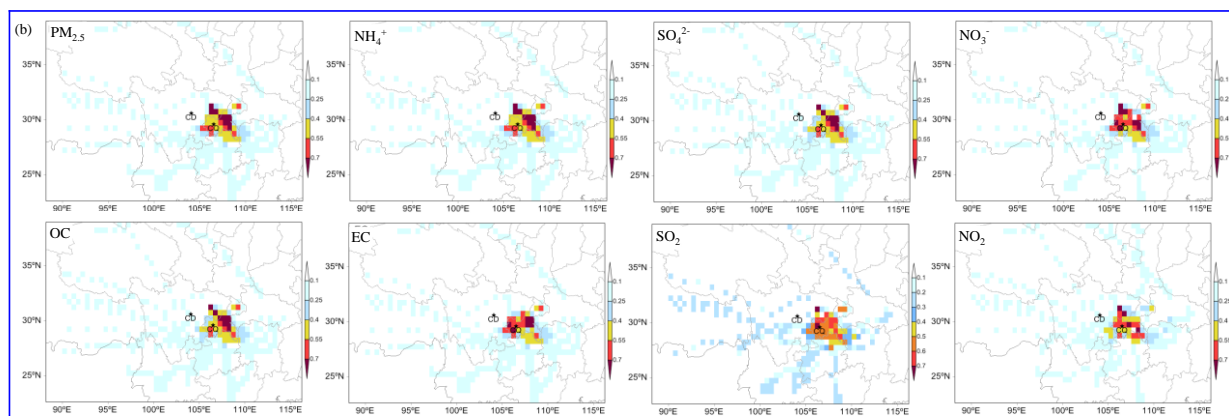
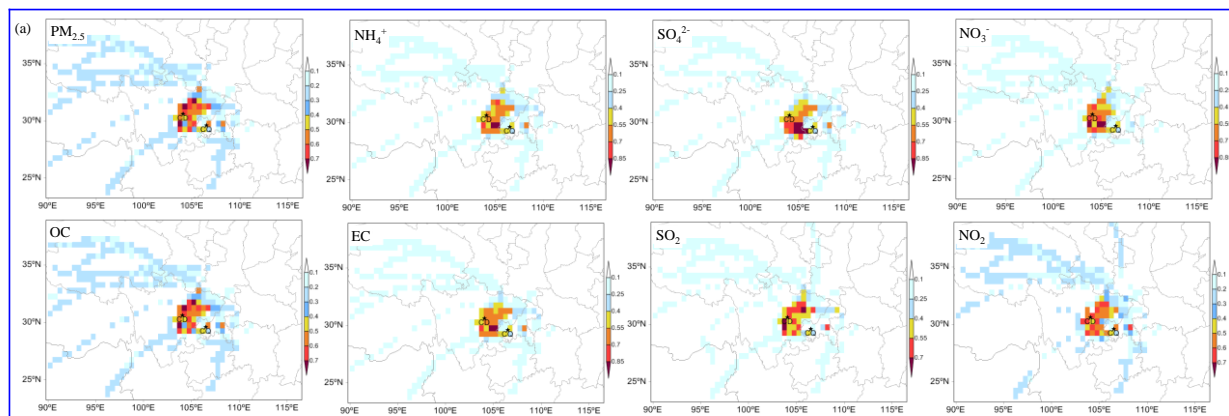


Figure 10. PSCF distribution of $\text{PM}_{2.5}$, its chemical components, and gaseous precursors in winter at CD (a) and CQ (b).